Co-published by
Institute of Fluid-Flow Machinery
Polish Academy of Sciences
Committee on Thermodynamics and Combustion
Polish Academy of Sciences

http://www.imp.gda.pl/archives-of-thermodynamics/

Thermomagnetic convection and entropy generation in a hybrid nanofluid filled wavy-walled cavity heated non-uniformly

Nirmalendu Biswas[a], Dipak Kumar Mandal[b*], Nirmal K. Manna[c], Ali Cemal Benim[d]

[a]Department of Power Engineering, Jadavpur University, Salt Lake, Kolkata-700106, India
[b]Department of of Mechanical Engineering, Government Engineering College Samastipur, Bihar-848127, India
[c]Department of Mechanical Engineering, Jadavpur University, Kolkata-700032, India
[d]Department Mechanical and Process Engineering, Duesseldorf University of Applied Sciences, Germany
*Corresponding author email: dipkuma@yahoo.com

Received: 31.03.2024; revised: 24.09.2024; accepted: 06.12.2024

Abstract

In this work, thermomagnetic convection and irreversibility production in a hybrid nanofluid-filled wavy-walled porous thermal system containing a semi-circular heated bottom is presented. Both the sidewalls of the enclosure are cooled and undulated with varying undulation numbers. The lower wall is partially undulated following a semi-circular-shaped object and is heated isothermally. The horizontal walls are insulated. The cavity is occupied with Cu-Al_2O_3/water-based hybrid nanofluid and porous substances under the impact of the evenly applied horizontal magnetic field. This work significantly contributes to the existing research rendering an exhaustive understanding of the hydrothermal flow-physics as well as irreversibility production of a hybrid nanofluid in the cavity having surface undulation. The Galerkin weighted finite element method is utilized to solve the mathematical model. The hydrothermal performance of the thermal system is considerably influenced by various pertinent factors such as Darcy-Rayleigh number, Darcy number, Hartmann number, and number of undulations. The wall undulations have a critical role in altering the hydrothermal performance. Heatlines are used to analyse heat transport dynamics from the protruded hot surface to the heat sink. The protruded heater wall induces the formation of a hot upward plume in the nearest fluid layers. The flow divides into two parts forming a pair of circulations due to symmetrical cooling at the sidewalls. The flow behaviours are significantly dampened by increasing the Hartmann number. The associated total entropy generation is also demonstrated. This study contributes to the existing domain knowledge and provides insights for designing and optimizing similar thermal systems.

Keywords: Magnetohydrodynamic flow; Nanofluid flow; Hybrid wavy-wall heating; Entropy generation; Heat transfer

Vol. 46(2025), No. 1, 61–81; doi: 10.24425/ather.2025.154182

Cite this manuscript as: Biswas, N., Mandal, D.K., Manna, N.K., & Benim, A.C. (2025). Thermomagnetic convection and entropy generation in a hybrid nanofluid filled wavy walled cavity heated non-uniformly. *Archives of Thermodynamics*, 46(1), 61–81.

1. Introduction

The intriguing interplay of thermomagnetic convective phenomena and irreversibility generation within an undulated enclosure occupied with a hybrid nanofluid, subject to non-uniform heating, stands as a captivating challenge at the forefront of contemporary research in fluid dynamics and thermal sciences. This study delves into the captivating realm of magnetohydrodynamics (MHD), where magnetic fields influence the dynamics of fluids with electrical conductivity, particularly under the impact of temperature gradients. In the multifaceted arena of scientific exploration, this intersection of magnetic fields with fluid dynamics holds sway over a multitude of applications, each more intriguing than the last [1].

Nomenclature

A – amplitude, m
B – strength of magnetic field, N $A^{-1}m^{-2}$
c_p – specific heat, J $kg^{-1}K^{-1}$
Da – Darcy number
Ec – Eckert number
F_c – Forchheimer constant
g – gravitational acceleration, m^2/s
H – length scale, cavity height, m
Ha – Hartmann number
k – thermal conductivity, W $m^{-1}K^{-1}$
K – porous medium permeability, m^2
L – length of enclosure, m
n – undulation number
NS – dimensionless entropy generation
Nu – Nusselt number (average)
p – pressure, Pa
P – dimensionless pressure
Pr – Prandtl number
Ra – Rayleigh number (fluid-based)
Ra_m – Darcy-Rayleigh number
S – entropy generation, W $m^{-3}K^{-1}$
T – temperature, K
u, v – velocity components, m s^{-1}
U, V – dimensionless velocity components
x, y – Cartesian coordinates, m
X, Y – dimensionless Cartesian coordinates

Greek symbols

α – thermal diffusivity, m^2 s^{-1}
β – coefficient of thermal expansion, K^{-1}
ε – porosity
θ – dimensionless temperature
λ – undulation amplitude
μ – dynamic viscosity, N $m^{-2}s$
ν – kinematic viscosity, m^2 s^{-1}
Π – heat function
ρ – density, kg m^{-3}
σ – electrical conductivity, μS cm^{-1}
φ – hybrid nanoparticles concentration
ψ – stream function

Subscripts and Superscripts

a – ambient
c – cold
d – dissipation
f – base fluid
gen – generation
h – hot
c – cold
loc – local
mf – magnetic
min – minimum
max – maximum
r – property ratio
s – solid
tg – thermal gradient
tot – total
vd – viscous

Abbreviations and Acronyms

MHD – magnetohydrodynamics

Magnetic fields can be harnessed to control and manage the transport of heat, momentum, and mass in multiphysical systems [2]. When magnetic fields are applied to fluid flows, they can alter local fluid velocities and modify the underlying flow physics. This is particularly relevant when dealing with complex systems that involve porous materials and nanofluids or hybrid nanofluids, which are colloidal mixtures of suspended nanoparticles in a base fluid [3].

The application of magnetic fields finds use in a wide array of modern technologies and industries [4]. For instance, it plays a crucial role in microfluidic devices [5], the manufacturing of crystals, electronic circuit cooling [6], heat exchange units, anti-vibrating systems, and molten metal flow regulators in nuclear reactors [7]. Moreover, magnetic fields have revolutionized medical science [8], contributing to advancements in specific medicine transport, cancer therapy and tumour treatment, magnetic endoscopy, control of blood flow during operation, gastrointestinal complaint management, biological waste transportation, and more [9].

Magnetothermally controlled systems work in complicated environments with porous media, hybrid nanofluids, and thermal gradients in many sophisticated applications [10]. The geometry and boundary conditions of these systems play a critical role in their design and analysis [11]. Surface undulation or corrugation, which enhances the surface area, can significantly influence near-wall transport processes, thereby altering the thermo-flow behaviour within thermal systems [12]. Researchers have tackled the modelling and analysis of such systems, which become even more challenging in the presence of porous structures and nanofluids or hybrid nanofluids. For instance, studies have investigated free convection in wavy-walled enclosures with varying undulation numbers, with varying results depending on the specific conditions [13]. Investigations into buoyancy-driven thermal convection flow in porous cavities having undulated walls that produce heat have similarly shown an increasing trend in heat transfer with an increase in the number and peak of the undulations [14]. Because of their improved thermal conductivity, hybrid and nanofluids have become more and more common [15]. This makes them useful in a variety of applications, even when flow-hindering porous materials exist [16]. Sarkar et al. presented a detailed overview of the developments of hybrid nanofluids [17]. A detailed review of the heat transfer enhancement utilizing nanofluid flow through a porous medium has been presented by Kasaeian et al. [18]. Several researchers have also studied the impact of surface morphology on the enhanced heat transfer in the presence of hybrid nanofluid [19,20], magnetic field [21,22], and others. Very recently Bahmani et al. [23] numerically studied the MHD buoyant convec-

tive process in different wavy-walled cavities packed with porous substances and reported the enhanced heat transfer with the existence of a curved surface.

Hamid et al. [24] in a recent study, examined the thermal convection in a cavity having curvilinear hot corners and with the existence of a central circular heated cylinder. They found enhanced heat transfer up to 400% when the heated cylinder radius increased. Pandit et al. [25] studied the impact of partial wavy walls on the hydrothermal convection of hybrid nanofluid in a porous cavity with the existence of multi-segmented magnetic fields. They achieved notably enhanced heat transfer up to 38% compared to traditional cavity. Better fluid mixing is made possible by the increased surface area and broken thermal boundary layers. The application of a segmented magnetic field with strategic orientation may lead to heat transfer enhancements of up to 26%. Guedri et al. [26] analysed the effect of wall waviness of a trapezoidal porous container filled with (multi-walled carbon nanotube-Fe_3O_4/water (MWCNT-Fe_3O_4/water) hybrid nanofluid under MHD effects on the heat transport phenomena. They achieved 26% enhanced heat transfer due to the increase in permeability. Mandal et al. [27] examined the impact of surface undulations on the convective heat transport in a porous cavity filled with hybrid nanofluid subjected to non-uniform multi-frequency heating and magnetic field. They found that at higher frequencies, heat transport increases up to 261.49%. Furthermore, compared to without undulations, an increase in the undulation height of the wavy sidewalls results in 13.41% enhanced heat transfer. In a corrugated porous cavity packed with Ag-MgO hybrid nanofluid, Al-Dulaimi et al. [28] studied the enhanced conjugate thermal convection. Further details could be found in [29,30]. In fact, current research has shown that increasing surface undulation does not always lead to improved heat transfer, highlighting the complexity of the relationship between undulation and heat transfer enhancement [31].

In this context, the current study investigates the behaviour of hybrid nanofluids in a confined cavity having surface undulations and the influence of a magnetic field. The study aims to shed light on how multiphysical factors, such as porous structure, nanofluids, and magnetizing fields, interact in irregular geometries. The cavity has an adiabatic top wall, wavy sidewalls that allow for cooling, and a partially heated bottom. The left sidewall receives the magnetic field applied perpendicularly. We alter a number of flow-regulating factors, such as the concentration of hybrid nanoparticles, the length of the active heating length, the strength of the magnetic field, the Darcy-Rayleigh number, and the Darcy number. This study contributes to our understanding of complex multiphysical phenomena in irregular geometries, offering insights that may find practical applications in solar thermal systems, thermal mixing processes, biomedical systems, and more. It is worth noting that this work differs significantly from our earlier studies, as it explores the impact of partial magnetic fields in a novel and previously unexplored geometry.

2. Problem geometry and mathematical modelling

The geometry under consideration is a two-dimensional wavy-walled enclosure, as illustrated in Fig. 1. This square-shaped enclosure has a length, denoted as L, and a height, denoted as H. Both the sidewalls of the cavity is not straight; it follows a wavy pattern described by the expression

$$y = 0.5A[1 - \cos(2n\pi y)], \quad (1)$$

where A and n denote the amplitude and wavy undulation number, respectively. The wavy walls are subject to isothermal cooling at a temperature T_c. The heating element is located on the central semicircular part of the bottom wall. The straight portions and the top horizontal wall are insulated.

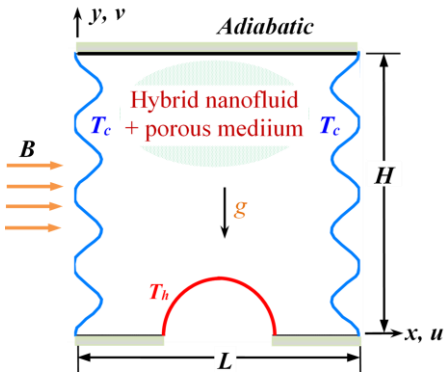

Fig. 1. The schematic illustration of the thermal system and boundary conditions.

This thermal system incorporates a hybrid nanofluid, a unique mixture consisting of Cu-Al_2O_3 nanoparticles dispersed within a host fluid. These nanoparticles are identical, spherical in shape, and have an average diameter of approximately 1 nm. The concentration of these nanoparticles within the hybrid nanofluid is maintained at a level below 3%. Importantly, following prior research [31], we ensure that there is no agglomeration or sedimentation of these nanoparticles within the fluid. The host fluid, in our case, is water, characterized by a Prandtl number (Pr) of 5.83. Furthermore, the porous medium is modelled utilizing the Forchheimer-Brinkman-Darcy model [32,33]. To simplify the mathematical model and ensure its practicality, we make several key assumptions:

- The magnetic Reynolds number (induced) is still very small, particularly at lesser concentrations of nanoparticles and lower magnetic field intensities. Because of this, the effects of induced magnetic fields, displacement currents, Joule heating, and the Hall effect are neglected [34].
- We also neglect the impact of radiative heat transfer and viscous dissipation effect, in line with earlier studies [35].

These assumptions allow us to focus on the primary thermomagnetic convection and entropy generation phenomena within our system, facilitating a more tractable mathematical model and a deeper understanding of the core dynamics.

The governing equations of continuity, momentum, and energy equations can be obtained in the dimensional form as follows, presuming the previously stated assumptions:

$$(X,Y)=(x,y)\frac{1}{H},\quad (U,V)=(u,v)\frac{H}{\alpha_f},$$
$$\theta=\frac{T-T_c}{T_h-T_c},\quad P=\frac{(p-p_a)H^2}{\rho\alpha_f^2}, \tag{2a}$$

$$\mathrm{Pr}=\frac{\nu_f}{\alpha_f},\ \mathrm{Da}=\frac{K}{H^2},\ F_c=\frac{1.75}{\sqrt{150\varepsilon^3}},$$
$$\mathrm{Ra_m}=\frac{g\beta_f(T_h-T_c)KH}{\nu_f\alpha_f},\ \mathrm{Ha}=BH\sqrt{\frac{\sigma_f}{\mu_f}}. \tag{2b}$$

The following dimensionless equations [34,35] are the resultant converted equations stated as

$$\frac{\partial U}{\partial X}+\frac{\partial V}{\partial Y}=0, \tag{3}$$

$$\frac{1}{\varepsilon^2}\left(U\frac{\partial U}{\partial X}+V\frac{\partial U}{\partial Y}\right)=-\frac{\partial P}{\partial X}+\frac{\nu}{\nu_f}\frac{\mathrm{Pr}}{\varepsilon}\left(\frac{\partial^2 U}{\partial X^2}+\frac{\partial^2 U}{\partial Y^2}\right)+$$
$$-\left(\frac{\nu}{\nu_f}\frac{\mathrm{Pr}}{\mathrm{Da}}+\frac{F_c\sqrt{U^2+V^2}}{\sqrt{\mathrm{Da}}}\right)U, \tag{4}$$

$$\frac{1}{\varepsilon^2}\left(U\frac{\partial V}{\partial X}+V\frac{\partial V}{\partial Y}\right)=-\frac{\partial P}{\partial Y}+\frac{\nu}{\nu_f}\frac{\mathrm{Pr}}{\varepsilon}\left(\frac{\partial^2 V}{\partial X^2}+\frac{\partial^2 V}{\partial Y^2}\right)+$$
$$-\left(\frac{\nu}{\nu_f}\frac{\mathrm{Pr}}{\mathrm{Da}}+\frac{F_c\sqrt{U^2+V^2}}{\sqrt{\mathrm{Da}}}\right)V+ \tag{5}$$
$$-\frac{\rho_f}{\rho}\frac{\sigma}{\sigma_f}\mathrm{Ha}^2\,\mathrm{Pr}\,V+\frac{\rho_f}{\rho}\frac{\beta}{\beta_f}\mathrm{Ra_m}\frac{\mathrm{Pr}}{\mathrm{Da}}\theta,$$

$$\left(U\frac{\partial\theta}{\partial X}+V\frac{\partial\theta}{\partial Y}\right)=\frac{\alpha}{\alpha_f}\left(\frac{\partial^2\theta}{\partial X^2}+\frac{\partial^2\theta}{\partial Y^2}\right). \tag{6}$$

The boundary conditions related to transport equations (3) through (6) are assumed to be $\theta = 1$ and $\theta = 0$, respectively, $\partial\theta/\partial Y=0$ at the cavity's horizontal walls, left and right walls, and zero velocity ($U = V = 0$) for each boundary wall.

The working medium (Cu-Al_2O_3/water hybrid nanofluid) comprises host fluid (water), and Al_2O_3 and Cu nanoparticles. The concentration φ designates the volume-based presence of the nanoparticles. The properties of the liquid phase and the two distinct types of nanoparticles (Al_2O_3 and Cu) are presented in Table 1 [36].

Table 1. Characteristics of Al_2O_3 and Cu nanoparticles and water [36].

Parameter	Unit	Water	Al_2O_3	Cu
α	$m^2\,s^{-1}$	1.47×10^{-7}	131.7×10^{-7}	1.11×10^{-4}
β	K^{-1}	21×10^{-5}	0.85×10^{-5}	1.67×10^{-5}
c_p	$J\,kg^{-1}K^{-1}$	4179	765	385
k	$W\,m^{-1}K^{-1}$	0.613	40	401
ρ	$kg\,m^{-3}$	997.1	3970	8933
μ	$kg\,m^{-1}s^{-1}$	9.09×10^{-4}	–	–

The thermal properties of the hybrid nanofluid are computed based on experimental models and empirical correlations, as shown in Table 2. Here, the combination of nanoparticles (Cu and Al_2O_3) and the host fluid (water) are signified by the symbols *s* and *f*, respectively. Additionally, the expression for dynamic viscosity, and thermal and electrical conducting properties [35] are incorporated in accordance with the traditional theoretical models. Nevertheless, the Brinkman model and the Maxwell model, two traditional expressions for thermal conductivity and viscosity, are unable to adequately forecast these characteristics for the hybrid nanofluids [36]. As shown in Table 3, precise values for the Cu-Al_2O_3/water hybrid nanofluid's thermal conductivity and viscosity are used from the experiments [36] to solve the aforementioned drawbacks.

In the post-processing stage, the solved primitive variables (U, V, θ) are used to produce several relevant dimensionless values. Based on an entropy generation (S_{gen} or NS_{gen}) analysis, the systems' deviation from ideal operation (reversible) is assessed.

Table 2. Relationships for the hybrid nanofluid Cu-Al_2O_3/water properties [35].

Thermodynamic properties	Relationships
Density (ρ)	$\rho=(1-\varphi)\rho_f+\varphi\,\rho_s$
Thermal conductivity (k)	$k=k_f\left[\frac{(k_s+2k_f)-2\varphi(k_f-k_s)}{(k_s+2k_f)+\varphi(k_f-k_s)}\right]$
Thermal diffusivity (α)	$\alpha=\frac{k}{\rho c_p}$
Electrical conductivity (σ)	$\sigma=\sigma_f\left[1+\frac{3\left(\frac{\sigma_s}{\sigma_f}-1\right)\varphi}{\left(\frac{\sigma_s}{\sigma_f}+2\right)-\left(\frac{\sigma_s}{\sigma_f}-1\right)\varphi}\right]$
Thermal expansion coefficient ($\rho\beta$)	$(\rho\beta)=(1-\varphi)(\rho\beta)_f+\varphi\,(\rho\beta)_s$
Specific heat capacity (ρc_p)	$(\rho c_p)=(1-\varphi)(\rho c_p)_f+\varphi(\rho c_p)_s$
Viscosity (μ)	$\mu=\frac{\mu_f}{(1-\varphi)^{2.5}}$

Magnetic field effects, fluid flow, and temperature gradient are all present in the current systems. As a result, irreversibility falls into three categories: irreversibility caused by thermal gradients (S_{tg} or NS_{tg}), irreversibility caused by fluid friction (viscous dissipation) (S_{vd} or NS_{vd}), and irreversibility caused by magnetic fields (S_{mf} or NS_{mf}). Here are the equations for the local irreversibility production rate (S_{gen} and NS_{gen}) as well as the dimensional (S) and dimensionless (NS) influences [34]:

$$S_{gen}=S_{tg}+S_{vd}+S_{mf}=\overbrace{\frac{k}{T^2}\left[\left(\frac{\partial T}{\partial x}\right)^2+\left(\frac{\partial T}{\partial y}\right)^2\right]}^{S_{tg}}+$$
$$+\overbrace{\frac{\mu}{T}\left[2\left(\frac{\partial u}{\partial x}\right)^2+2\left(\frac{\partial u}{\partial y}\right)^2+\left(\frac{\partial u}{\partial y}+\frac{\partial v}{\partial x}\right)^2\right]}^{S_{vd}}+\overbrace{\frac{\sigma B^2}{T}v^2}^{S_{mf}}, \tag{7}$$

$$NS_{gen}=\frac{S_{gen}}{\frac{k_f}{H^2}}=NS_{tg}+NS_{vd}+NS_{mf}=$$

$$= \overbrace{\frac{1}{(\theta+\theta_r)^2}\frac{k}{k_f}\left[\left(\frac{\partial\theta}{\partial X}\right)^2+\left(\frac{\partial\theta}{\partial Y}\right)^2\right]}^{NS_{tg}} + \\ + \frac{\mathrm{EcPr}}{(\theta+\theta_r)}\frac{\mu}{\mu_f}\overbrace{\left[2\left(\frac{\partial U}{\partial X}\right)^2+2\left(\frac{\partial V}{\partial Y}\right)^2+\left(\frac{\partial U}{\partial Y}+\frac{\partial V}{\partial X}\right)^2\right]}^{NS_{vd}} + \\ + \overbrace{\frac{\mathrm{EcPrHa}}{(\theta+\theta_r)}\frac{\sigma}{\sigma_f}V^2}^{NS_{mf}}. \quad (8)$$

Equation (8) includes the Eckert number (Ec) and the temperature ratio reference parameter (θ_r), which are specified as

$$\theta_r = \frac{T_c}{T_h - T_c}, \quad (9)$$

$$\mathrm{Ec} = \frac{\alpha_f^2}{H^2 c_{pf}(T_h - T_c)} = \sqrt[3]{\frac{(g\alpha_f\beta_f)^2}{T_h - T_c}}\,\mathrm{Pr}^{-\frac{2}{3}}\mathrm{Ra}^{-\frac{2}{3}}. \quad (10)$$

One possible global characteristic of the systems is their total entropy generation (NS_{tot}). It is calculated as the result of integrating the generation of local entropy over the whole flow domain:

$$NS_{tot} = \iint NS_{gen}\,dX\,dY. \quad (11)$$

Using the local and average Nusselt numbers (Nu), which are provided by, the heated wavy wall's average and local rates of heat transfer:

$$\mathrm{Nu}_{loc} = \frac{k}{k_f}\left(-\frac{\partial\theta}{\partial n}\Big|_{hw}\right), \quad (12a)$$

$$\mathrm{Nu} = \frac{k}{k_f}\frac{1}{s}\int_0^s\left(-\frac{\partial\theta}{\partial n}\Big|_{hw}\right)dS, \quad (12b)$$

where s stands for both the appropriate coordinate point and the real length of the wavy wall. Streamlines are used to graphically represent localized fluid flow patterns inside flow geometries. The stream function (ψ) is used to generate streamlines from the solved velocity field. The expression for the stream function is

$$-\frac{\partial\psi}{\partial X} = V \quad \text{and} \quad \frac{\partial\psi}{\partial Y} = U. \quad (13)$$

3. Numerical technique

The finite element method (FEM) is employed to discretize the transport equations. The method of solving the equations is iterative and continues until the residuals meet a predetermined convergence threshold, usually set at a strict level so that the residuals are $\leq 10^{-6}$. This methodology conforms to accepted procedures in the field and guarantees the simulations' correctness and stability [31,35]. The flexible finite element analysis program offers a reliable foundation for resolving challenging multiphysics issues. It is the perfect fit for this study because of its ability to handle linked physical phenomena like heat transfer, fluid flow, and magnetic fields with ease. Because of this meticulous selection, the computational investigations have a solid foundation in precise and confirmed data, which supports the numerical model.

Prior research has thoroughly validated the accuracy and dependability of the selected numerical approach [31,35]. These validations include a thorough evaluation of the computational outcomes in comparison to experimental data as well as cross-validation with other numerical simulations. The computational and experimental results are consistently observed, which highlights the resilience of the approach and validates the veracity of the simulated results.

Additionally, a thorough validation investigation is conducted by comparing the computed findings with the results of Ghasemi et al. [38] to validate our computational results. To assess the accuracy of numerical approaches for forecasting heat transfer for magnetohydrodynamic free convective process in the cavity, the present solver outcome is compared with the published results of Ghasemi et al. [38]. This work uses a horizontal magnetic field, an Al_2O_3/water nanoliquid, and a square geometry having heating and cooling from the vertical sides. The comparison is carried out for different values of Ha (= 0 − 60) and φ (= 0%, and 2%) at Ra = 10^5. The comparative results are shown in Table 3 using ψ_{max}. The two results of the comparison exhibit excellent agreement. These comparative assessments show that MHD-free convection in a confined cavity may be predicted using the current numerical technique.

Table 3. Comparing ψ_{max} of the present results and results of Ghasemi et al. [38] for varying Ha and φ at Ra = 10^5.

Ha	Ghasemi et al. [38]		Present simulation	
	φ = 0%	φ = 2%	φ = 0%	φ = 2%
0	11.053	11.313	11.014	11.275
30	5.710	5.682	5.693	5.878
45	3.825	3.729	3.813	3.922
60	2.518	2.518	2.614	2.677

In addition, a grid refinement test was methodically carried out to confirm that the grid size had no discernible impact on the numerical simulations. To guarantee the precision and dependability of the simulations, this test is essential. All of the geometric shapes that were used in the grid generation for the current two-dimensional challenges were created using the finite element method. However, in this study, a finer mesh structure is utilized for the extensive simulations, which provides the correct results. Hence, no mesh independence study is presented here.

4. Results and discussion

Here, we delve into the intricate thermal transport phenomena occurring within the cavity, characterized by wavy left and right walls, heated from the bottom in the form of a semi-circle, and subjected to the effect of an external flat magnetic field [39]. Our investigation unveils a rich tapestry of insights, with the results elucidated through the visualization of key parameters, including streamlines (ψ), isotherms (θ), heatlines (IT), and the average Nusselt number (Nu). We explore a wide range of controlling variables, spanning various undulation numbers (n = 1, 2, 4, 6, 8), Darcy-Rayleigh numbers ($1 \leq \mathrm{Ra_m} \leq 10^4$), Darcy numbers ($10^{-4} \leq \mathrm{Da} \leq 10^{-2}$), and Hartmann numbers ($0 \leq \mathrm{Ha} \leq 70$).

Furthermore, the irreversibility study as a result of fluid friction, thermal, and magnetic force are also assessed. The porosity and volumetric concentration of hybrid nanofluids are taken as $\varepsilon = 0.8$ and $\varphi = 0.1\%$.

4.1. Magneto-thermal transport structures

4.1.1. Flow signatures

Figure 2 encapsulates the flow signatures within the cavity, offering a visual narrative of how fluid dynamics evolve under different parameter regimes. The variations in wavy wall undulations (n = 1, 2, 4 and 6), Darcy-Rayleigh number (Ra_m = 10, 10^2, 10^3, 10^4), and Rayleigh number (Ra = 10^4, 10^5, 10^6, 10^7) are meticulously examined at Da = 10^{-3} and Ha = 10. Our observations reveal intriguing insights into the flow patterns within the cavity. Notably, as the Rayleigh number rises, the change from pure conduction dominance to convection mode becomes evident, manifesting as an increase in flow velocity. This transition is mainly marked in the presence of strong convection, where the flow velocity triples (as observed at Ra = 10^5 and 10^6).

The interplay of wavy wall undulations and Rayleigh numbers elucidates the impact of geometric configuration on flow behaviour. This exploration of basic flow patterns, as depicted in Fig. 2, lays the foundation for the in-depth investigations and analyses that follow in this study. These flow signatures serve as a critical reference point for our subsequent discussions and findings, shedding light on the underlying physics governing the system's response to varying parameters. Utilizing a half-circular wall at the centre of the bottom surface enhances the heating effect, while the elongated wavy walls contribute to an extended cooling surface. The central half-circular bottom heating results in an upward flow of heated water that returns over both wavy sidewalls. The presence of surface waviness at the sidewalls plays a pivotal role in altering the directions of flow velocity, leading to the formation of distinct circulation patterns. At lower Darcy-Rayleigh numbers, undulations have no remarkable im-

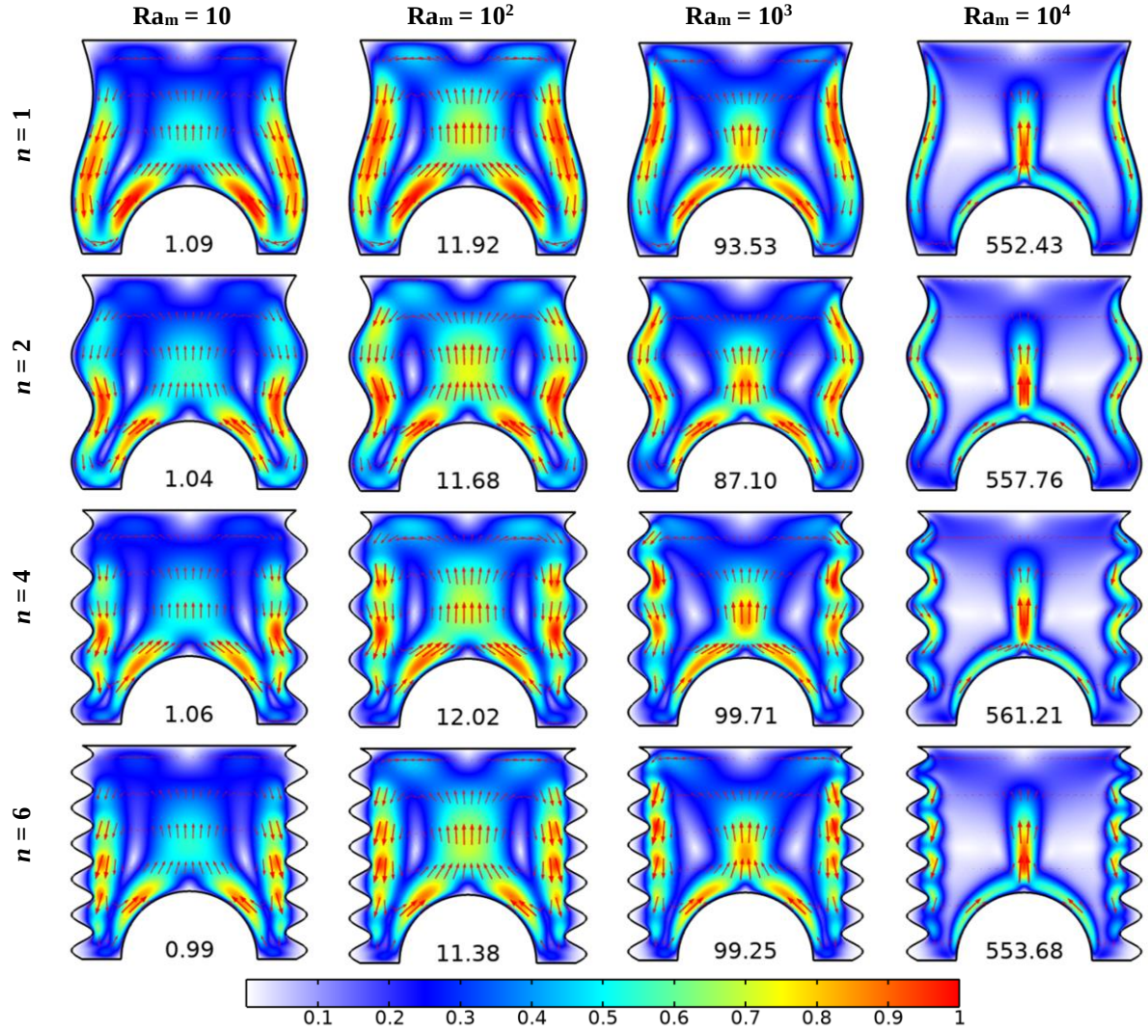

Fig. 2. Flow signatures varying with undulations (n = 1, 2, 4, and 6) and Darcy-Rayleigh numbers (Ra_m = 10, 10^2, 10^3, 10^4) at different Rayleigh numbers (Ra = 10^4, 10^5, 10^6, 10^7), for Da = 10^{-3}, Ha = 10. The value below each figure indicates maximum velocity (dimensionless).

pact on velocity magnitude. However, at higher Ra_m values, particularly for $n = 4$, a substantial increase in velocity is observed. A rise in Ra_m leads to a significant enhancement in flow velocity. This heightened velocity is particularly confined to the central region and adjacent to the wavy walls, reflecting the complex interplay of buoyancy-driven flow physics and geometric configuration.

4.1.2. Streamline evolution

Figure 3 provides a comprehensive view of the evolving flow circulation patterns within the cavity, allowing us to unravel critical insights into the system's behaviour under varying conditions. This analysis was conducted for various undulations (n = 1, 2, 4 and 6) and Darcy-Rayleigh numbers (Ra_m = 10, 10^2, 10^4) while keeping Darcy number fixed at 10^{-3} and Hartmann number at 30. It yields several noteworthy observations.

The formation of streamlines reveals the emergence of two symmetrical circulations within the cavity, indicative of the complex interplay between buoyancy-driven flow and geometric configuration. As the Darcy-Rayleigh number reaches 10^4, signifying the dominance of convection, the strength of these circulations intensifies significantly. This escalation in circulation strength is a hallmark of the transition from conduction to convection-dominated flow regimes. Interestingly, the presence of more undulations at the cold wavy walls leads to a phenomenon where flow stagnates at the vertical walls, causing a retardation in circulation strength. Consequently, an increase in the number of undulations results in a reduction in circulation

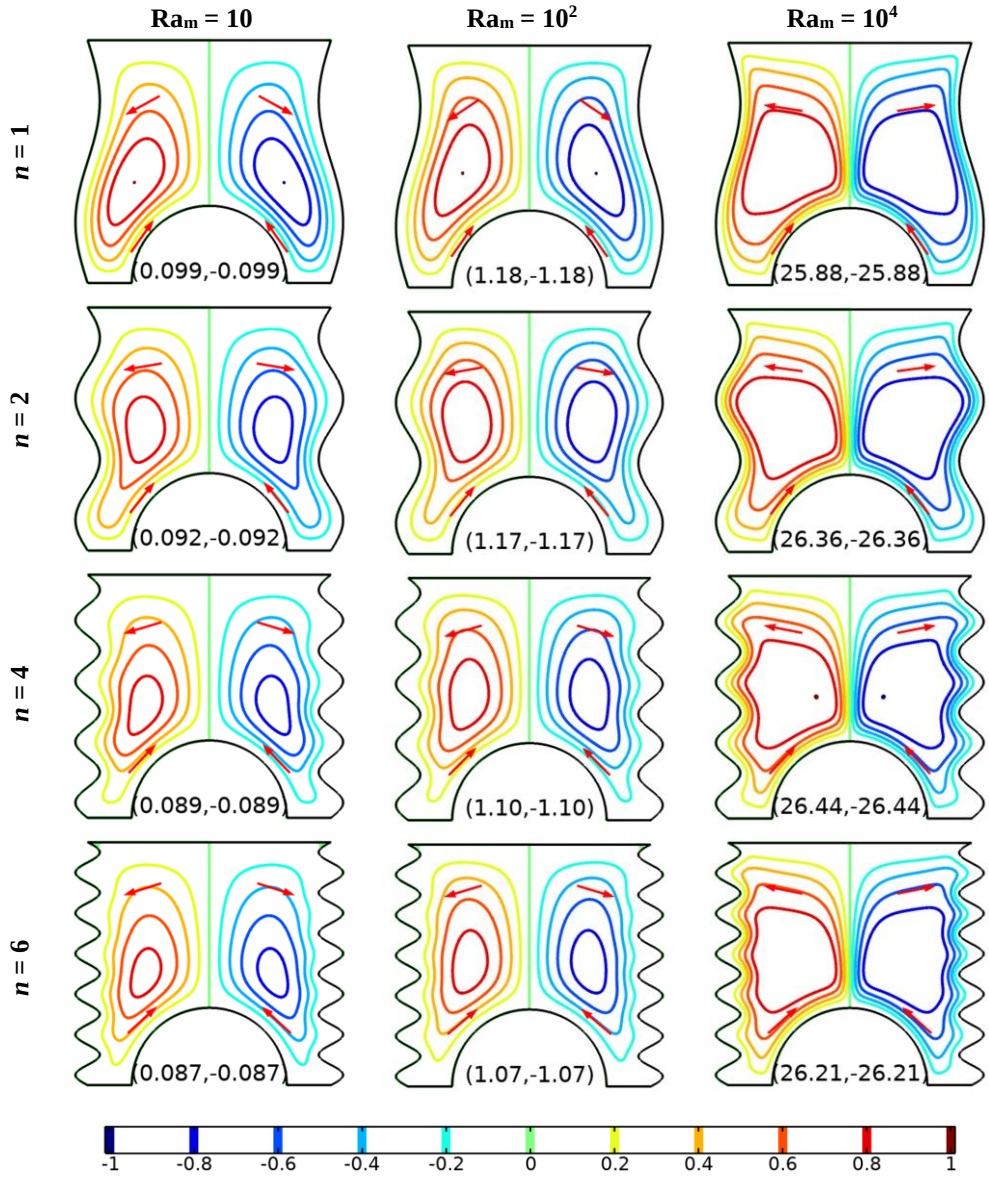

Fig. 3. Evolution of flow circulation at various undulations (n = 1, 2, 4 and 6) and Darcy-Rayleigh numbers (Ra_m = 10, 10^2 and 10^4), for Da = 10^{-3}, Ha = 30. The values below each figure indicate ψ_{max} and ψ_{min}, respectively.

strength. This effect is particularly pronounced at lower Ra_m values, emphasizing the intricate relationship between wall waviness and flow dynamics. In contrast, at higher Ra_m values, especially at $Ra_m = 10^4$, an intriguing phenomenon is observed. The circulation strength reaches an optimum value when the number of undulations is set at $n = 4$. This suggests that, under specific conditions, the presence of moderate wall undulations can enhance circulation strength, highlighting the subtle balance between geometric complexity and flow dynamics. These insights into streamline evolution offer a deeper understanding of how fluid circulations respond to varying parameters within the cavity. They underscore the role of convection dominancy, wall waviness, and the interplay of these factors in shaping circulation patterns and flow behaviour.

4.1.3. Isotherm evolution

Figure 4 presents a comprehensive depiction of the evolving isotherm patterns within the cavity, offering critical insights into the distribution of static temperature under varying conditions. This analysis was conducted for various undulations (n = 1, 2, 4 and 6) and Darcy-Rayleigh numbers (Ra_m = 10, 10^2, 10^4) while keeping Darcy number fixed at 10^{-3} and Hartmann number at 30, unveils several notable observations.

The formation of isotherms showcases intriguing behaviour. Initially, these isotherms assume a circular shape at the heating wall and gradually transform into elliptical patterns as they ascend toward the top wall. This transition from circular to elliptic isotherms reflects the complex interplay of heat transfer mecha-

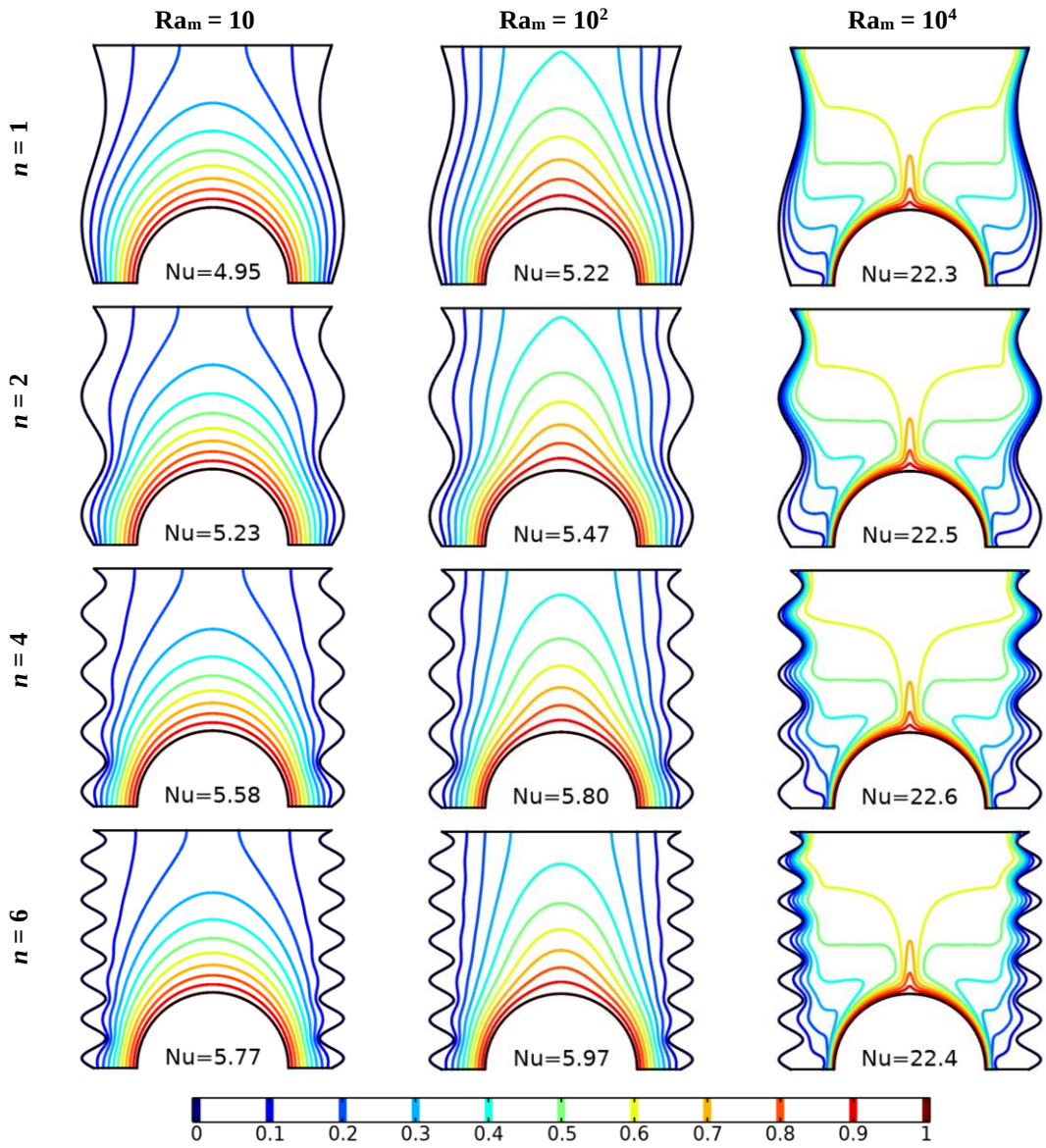

Fig. 4. Evolution of static temperature at various undulations (n = 1, 2, 4 and 6) and Darcy-Rayleigh numbers (Ra_m = 10, 10^2 and 10^4), for Da = 10^{-3}, Ha = 30.

nisms within the cavity. As the Darcy-Rayleigh number increases, signifying the onset of convection, a notable phenomenon emerges. The hot isotherms stratify horizontally over the top of the cavity, indicating a more efficient heat transfer process. This stratification is a clear indicator of enhanced heat transfer, leading to a rise in the Nusselt number. The presence of wavy cold walls further amplifies heat transfer, with increasing wavy undulations leading to an increase in the effective cold surface area. Consequently, the Nu value reaches its optimum at $Ra_m = 10^4$ when the number of undulations is set at $n = 4$.

However, an intriguing observation emerges when undulations are further increased. Beyond this optimum point, a reduction in heat transfer is noted. This phenomenon may be attributed to flow separation at the vertical walls, which disrupts the convective heat transfer process. These insights into isotherm evolution shed light on the complex dynamics of temperature distribution within the cavity. They underscore the role of convection, wall waviness, and their interplay in shaping temperature patterns and heat transfer efficiency. The findings also highlight the delicate balance between geometric complexity and heat transfer performance within this unique thermal system.

4.1.4. Magneto-thermofluid flow patterns

The Hartmann number, representing the influence of an external magnetic field that opposes the fluid flow, serves as a pivotal controlling parameter in this study. The profound alterations in flow physics induced by varying Ha values (Ha = 0, 50 and 70) are meticulously examined to understand the magnetic field's

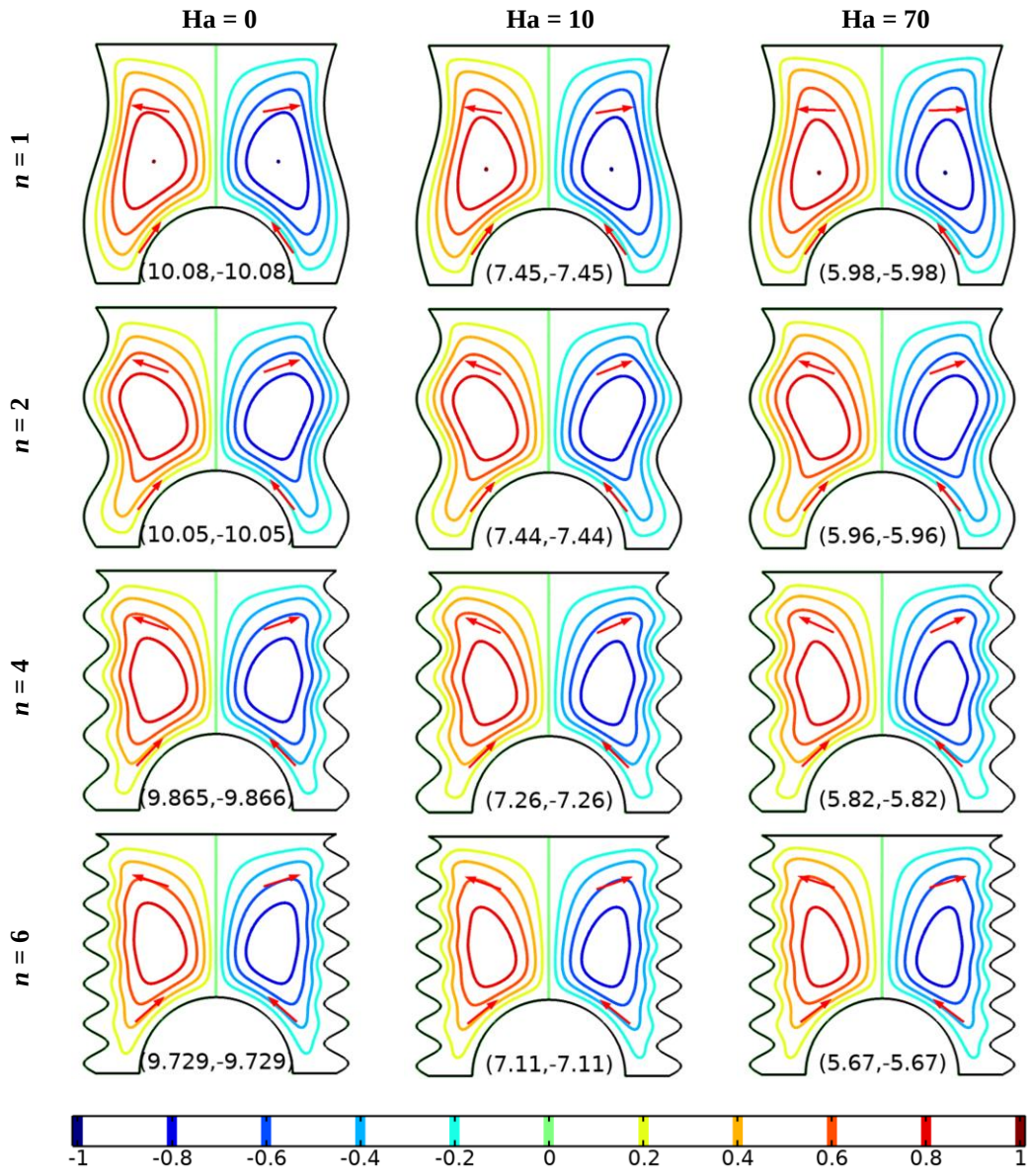

Fig. 5. Magnetic field (Ha) effect on the evolution of flow circulation at various undulations (n = 1, 2, 4 and 6), Hartmann number (Ha = 0, 10 and 70), for $Ra_m = 10^3$, $Da = 10^{-3}$. The values below each figure indicate ψ_{max} and ψ_{min}, respectively.

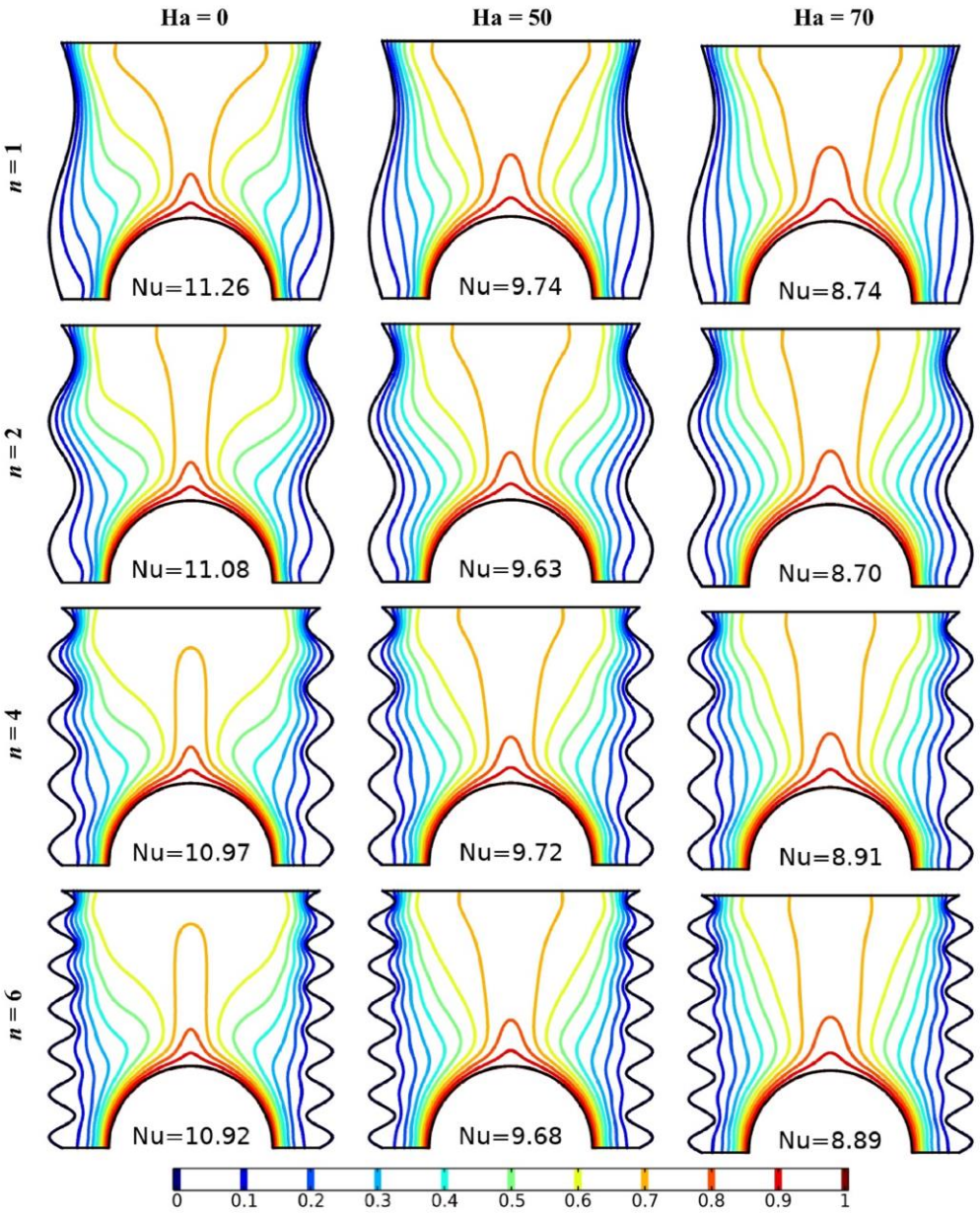

Fig. 6. Magnetic field (Ha) effect on the evolution of static temperature at various undulations (n = 1, 2, 4 and 6), Hartmann number (Ha = 0, 50 and 70) for $Ra_m = 10^3$, $Da = 10^{-3}$.

impact on the system's behaviour (as depicted in Fig. 5). It shows that, as Ha values increase, reflecting a stronger magnetic field's dampening effect on the flow, a noticeable change in flow dynamics unfolds. This effect is observed across different undulation numbers (n = 1, 2, 4 and 6). Secondly, the flow strength experiences a steady reduction with increasing Ha values. This phenomenon underscores the magnetic field's ability to restrain fluid motion, leading to diminished circulation within the cavity. Moreover, the magnetic field's influence extends to the distribution of static temperature within the cavity, as illustrated in Fig. 6. At the heated wall, isotherms become progressively thicker with the rise in Ha values. This phenomenon indicates that the magnetic field's presence results in a more pronounced impact (reducing local temperature gradient near the heater as well as cooler surfaces), affecting heat transfer patterns within the cavity. These observations emphasize the pivotal role of the Hartmann number in modulating flow circulation and temperature distribution within the system. The magnetic field's ability to alter flow strength and temperature gradients holds significant implications for the overall thermal performance of the cavity, particularly in scenarios where magnetohydrodynamics plays a critical role.

4.2. System analysis from design perspectives

In the pursuit of understanding the intricate thermal system from a design perspective, we delve into the profound influence of Darcy parameters, particularly the Darcy number, which characterizes the permeability of the porous medium and its resistance to fluid flow. To assess the impact of Da on fluid flow

physics, we examine its effects at Da = 10^{-4}, 10^{-3} and 10^{-2} (as depicted in Fig. 7). As we elevate the Da values, signifying a reduction in the porous medium's resistance to flow, a clear trend emerges — flow circulation within the cavity decelerates. This observation aligns with the fundamental physics of porous media, where lower Da values correspond to higher resistance and, consequently, slower fluid flow. Streamline contours, which are invaluable in revealing flow patterns, consistently exhibit symmetric behaviour across all combinations of the Darcy number and undulation parameter. The system exhibits two counter-rotating circulations, with fluid rising along the mid-vertical plane of this intricate thermal setup. However, the intriguing revelation here is that as Da increases from 10^{-4} to 10^{-2}, the circulation strength diminishes. This unexpected decline in flow rate with increasing Da at a constant modified Rayleigh number (the Darcy-Rayleigh number) is attributed to the reduction in fluid-based Rayleigh number. The Rayleigh number is inherently responsible for driving flow within the confined domain due to temperature gradients. This insight into the interplay between Da and flow circulation underscores the significance of porous media characteristics in shaping fluid dynamics within the cavity. Moreover, it highlights the nuanced relationship between resistance to flow and circulation strength – a critical consideration in optimizing the design of thermal systems with porous components. Turning the attention to the distribution of static temperature, we uncover additional insights into the impact of Da, as illustrated in Fig. 8. Isotherms, which provide valuable information about the mode of temperature transfer (convection or conduction), exhibit distinct behaviour as Da varies. At lower Da values (Da = 10^{-4}, 10^{-3}), isotherms exhibit intricate and wavy patterns, indicative of strong convection heat transfer.

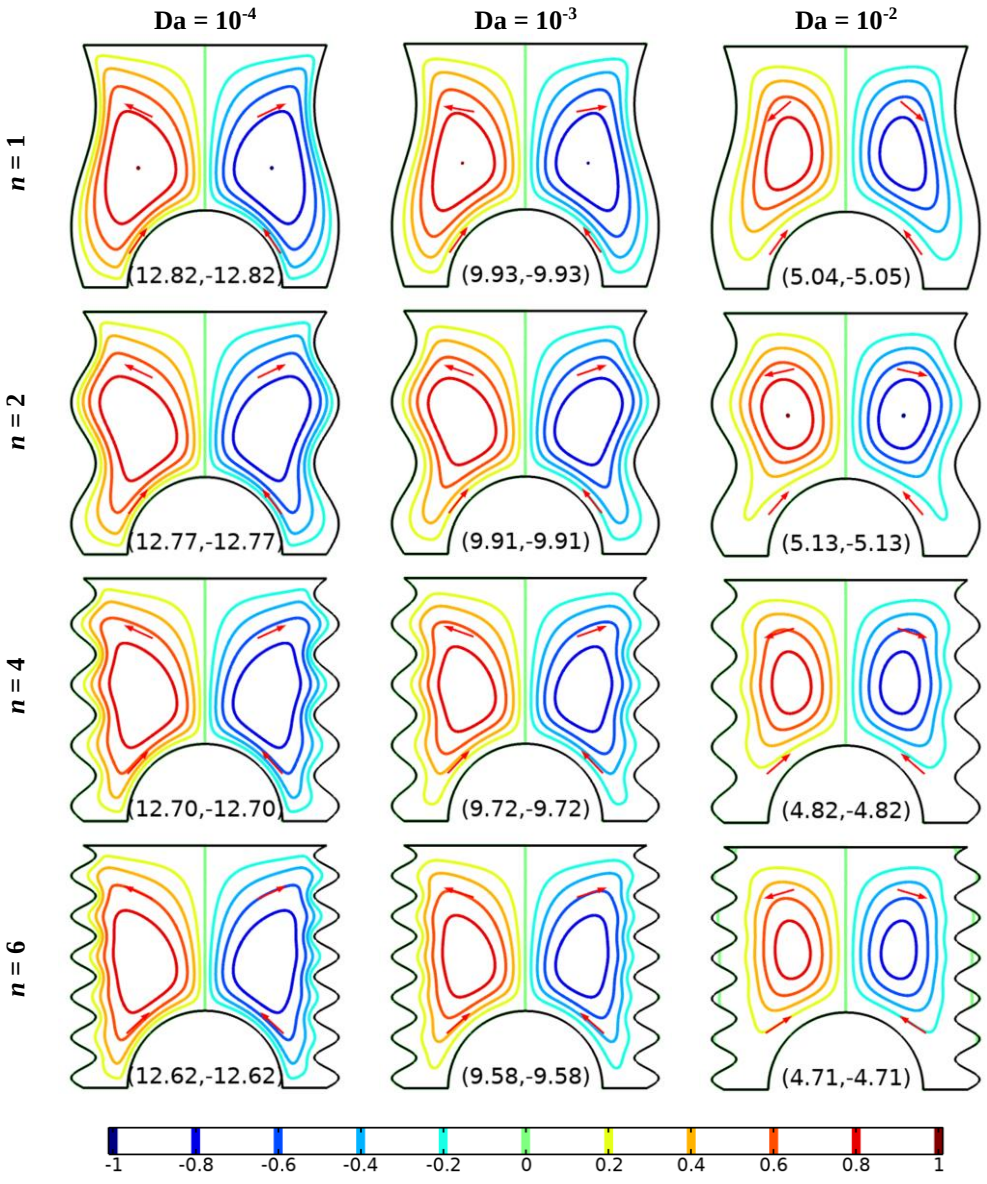

Fig. 7. Evolution of flow circulation at various undulations (n = 1, 2, 4 and 6) and Darcy numbers (Da = 10^{-4}, 10^{-3} and 10^{-2}), for $Ra_m = 10^3$, Ha = 10. The values below each figure indicate ψ_{max} and ψ_{min}, respectively.

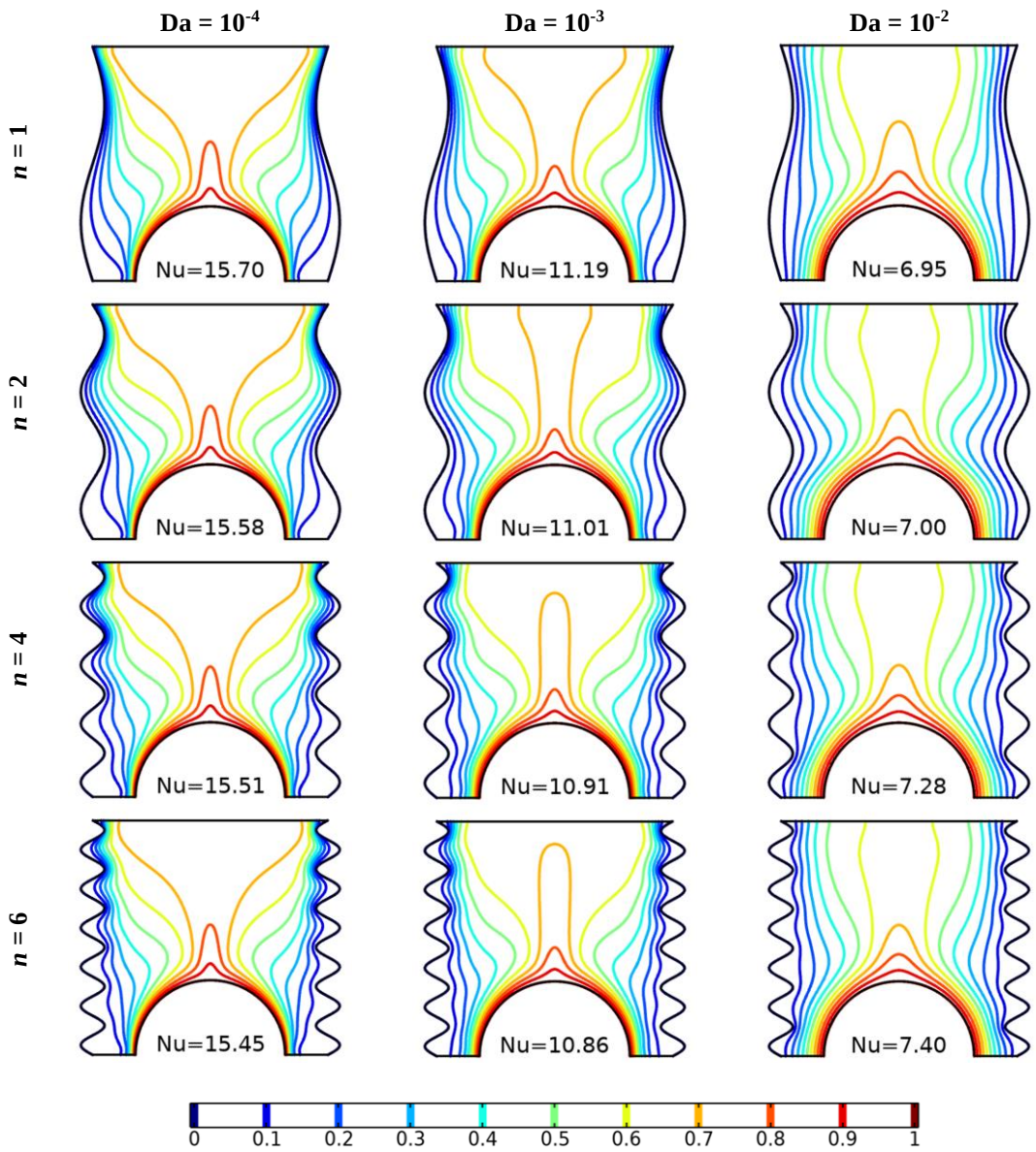

Fig. 8. Evolution of static temperature at various undulations (n = 1, 2, 4 and 6) and Darcy numbers (Da = 10^{-4}, 10^{-3} and 10^{-2}), for $Ra_m = 10^3$, Ha = 10.

As Da increases, isotherm contours spread more towards the top wall and become notably smoother. Additionally, the clustering of isotherms and streamlines over the lower portion of the semi-circular wall and the upper regions of the undulated sidewalls diminishes at higher Da values. This shift in thermal boundary layer dynamics impacts the local Nusselt number and normal temperature gradient, resulting in a significant reduction in the average Nusselt number, as indicated below the figures. The highest average Nu magnitude is observed at low Da values and sharply decreases as Da increases. These findings emphasize the intricate interplay between fluid flow, porous medium characteristics, and heat transfer within the cavity. They underscore the critical role of Da in shaping both flow and temperature distribution, offering valuable insights for the design and optimization of thermal systems involving porous media.

4.3. Heatline visualization

In the quest to unravel the intricate mechanisms of thermal energy transport within the cavity, we turn our attention to heatline visualization (as depicted in Fig. 9). This technique offers valuable insights into how thermal energy moves across different configurations of the system, characterized by varying Darcy-Rayleigh numbers and undulations (n), while maintaining a con-

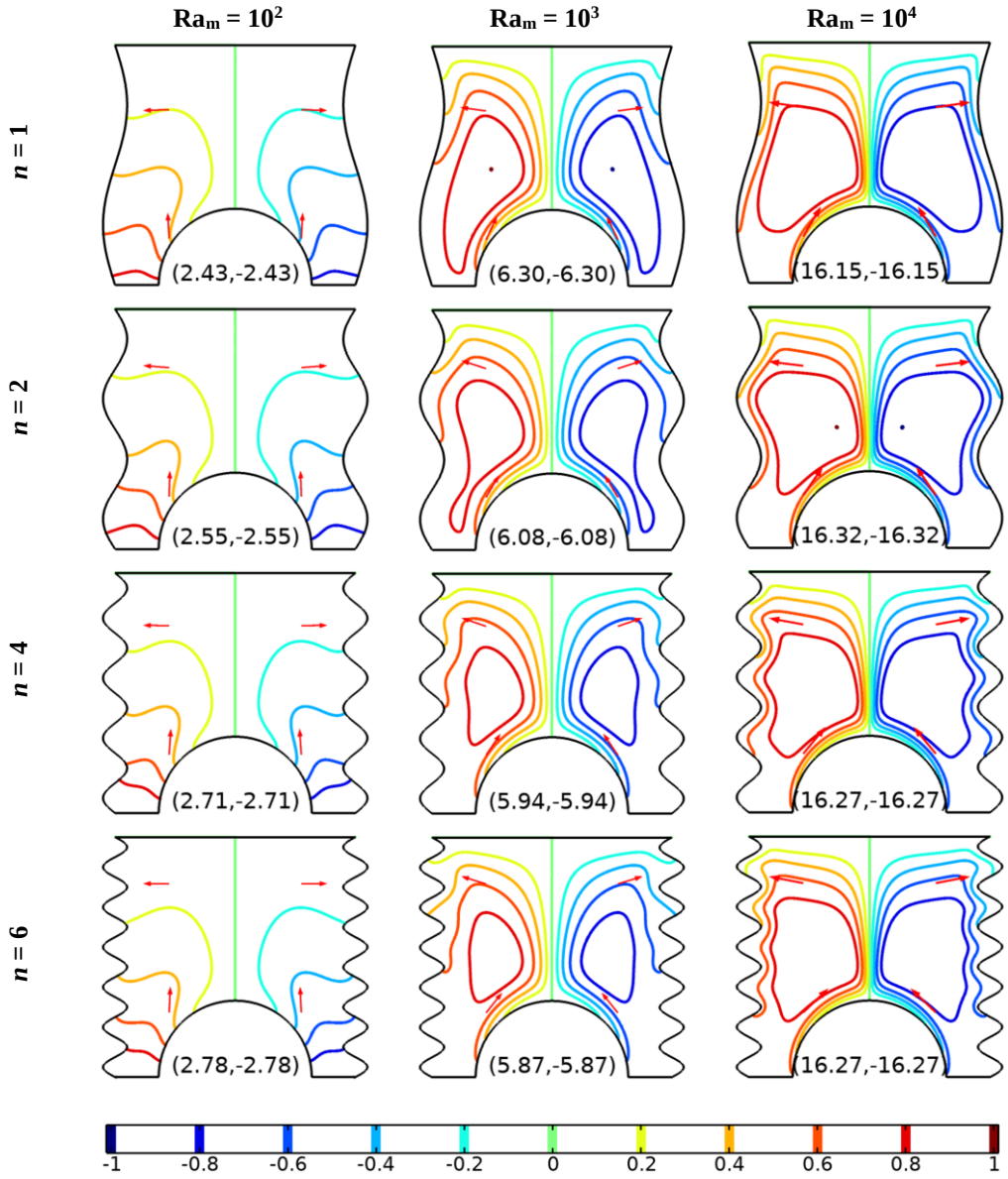

Fig. 9. Heatline visualization at various undulations (n = 1, 2, 4 and 6) and Darcy-Rayleigh numbers (Ra$_m$ = 10^2 to 10^4), for Da = 10^{-3} and Ha = 30. The values below each figure indicate Π_{max} and Π_{min}, respectively.

stant Darcy number (Da = 10^{-3}) and Hartmann number (Ha = 30).

As we manipulate Ra$_m$, a noticeable shift in the heat transport mechanism becomes apparent. At low Ra$_m$ values, heatlines exhibit straightforward paths from the hot wall to the cold wall, indicating a dominance of conduction-driven heat transfer. However, as Ra$_m$ increases, these heatlines disperse, tracing larger and more convoluted paths towards the cold wall. This transformation signifies a transition from conduction-dominated to convection-dominated heat transfer. Notably, at high Ra$_m$ values, two symmetrical circulations emerge within the cavity, driven by intensified convective forces. Furthermore, heatlines with varying undulations showcase enhanced energy transport from the hot wall, emphasizing the influence of wall waviness on thermal dynamics.

The impact of magnetic fields, quantified by the Hartmann number, on heatline patterns is explored in Fig. 10. We find that the magnetic damping effect causes the energy recirculations to diminish as Ha grows. In the absence of a magnetic field (Ha = 0), representing non-MHD flow, energy recirculations are more robust, resulting in the strongest heat flow. Conversely, as Ha rises to 50 or 70, energy circulation diminishes, leading to reduced heat transfers. Regions with congested heatlines indicate strong flowing heat flux, primarily located near the vertex of the semicircular heater.

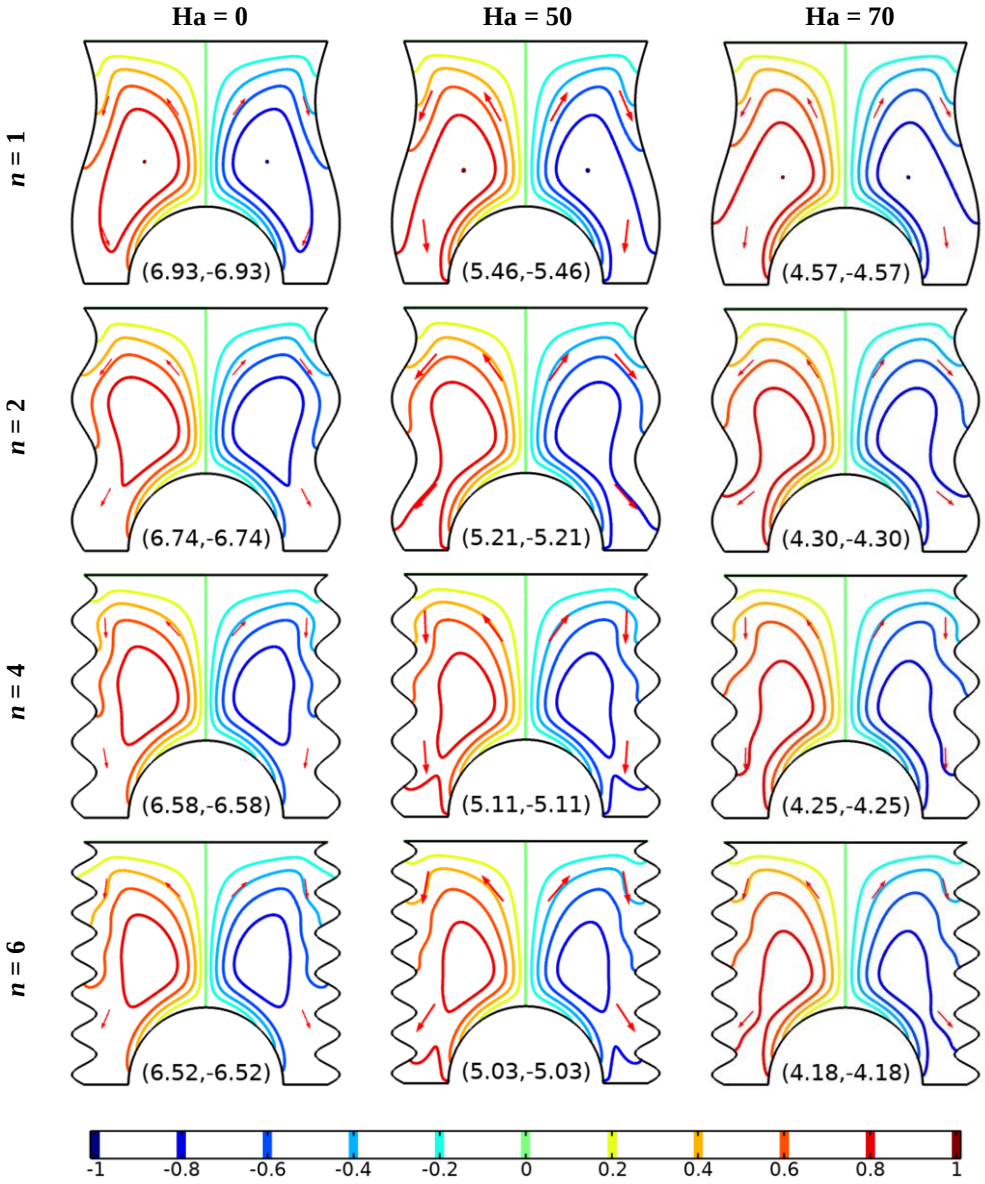

Fig. 10. Evolution of heatlines at various undulations (n = 1, 2, 4 and 6) and Hartmann numbers (Ha = 0, 50 and 70), $Ra_m = 10^3$, for $Da = 10^{-3}$. The values below each figure indicate Π_{max} and Π_{min}, respectively.

The investigation into the impact of the Darcy number on heatline patterns, while keeping $Ra_m = 10^3$ and Ha = 10 constant, reveals intriguing insights (as depicted in Fig. 11). Surprisingly, as Da increases, allowing for less-resisting flow, the heat flow within the system decreases. This counterintuitive observation contradicts the expectation that increased permeability, associated with higher Da values, should lead to enhanced heat flow. However, this behaviour aligns with our earlier streamline results, demonstrating the intricate interplay between porous medium characteristics, resistance to flow, and heat transfer. Notably, at $Da = 10^{-4}$, characterized by a high fluid-based Rayleigh number ($Ra = 10^7$), heatline contours exhibit greater magnitude, indicative of strong fluid circulation. At $Da = 10^{-2}$, a transitional behaviour emerges, bridging the gap between conduction-dominated and convection-dominated heat transfer.

4.4. Thermodynamic irreversibility generation

In pursuit of comprehending the intricate thermodynamic aspects of the system, we delve into the analysis of entropy generation, a fundamental parameter shedding light on the thermodynamic irreversibilities inherent to the thermal system. This analysis proves indispensable in understanding the efficiency and performance of the system under varying conditions, enabling

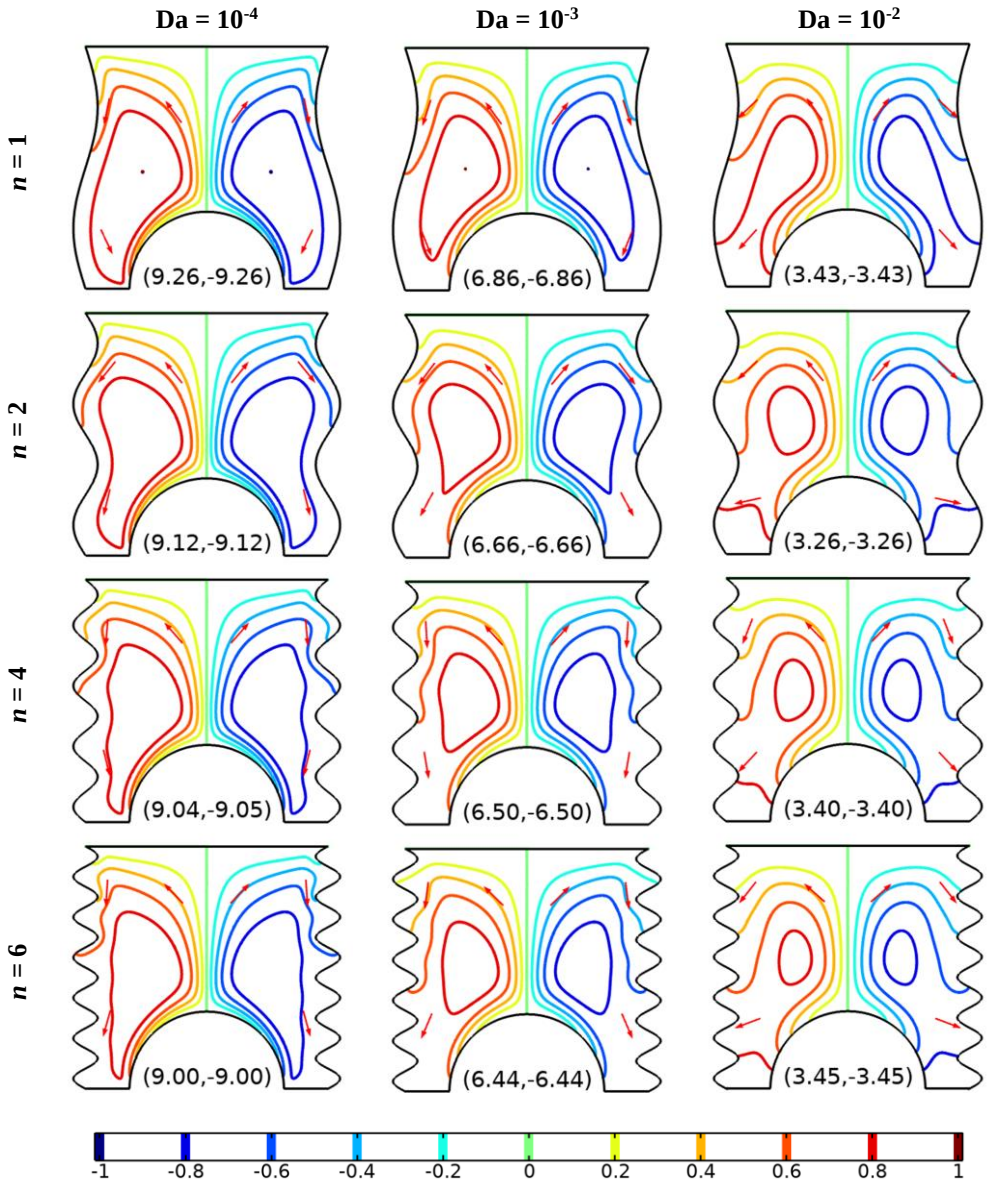

Fig. 11. Evolution of heatlines at various undulations (n = 1, 2, 4 and 6) and Darcy numbers (Da = 10^{-4}, 10^{-3}, 10^{-2}), for $Ra_m = 10^3$, for Ha = 10. The values below each figure indicate Π_{max} and Π_{min}, respectively.

us to make informed design choices. First and foremost, the examination of normalized local total irreversibility generation (*NS*) reveals intriguing insights, as depicted in Fig. 12. At lower Darcy-Rayleigh numbers ($Ra_m = 10^2$), *NS* is predominantly conduction-dominated, signifying the prevalence of heat transfer through conduction mechanisms. Interestingly, *NS* reaches its maximum in the vicinity of the heating and cooling zones within the cavity, gradually diminishing as one moves toward the top adiabatic wall. However, as Ra_m increases, transitioning the system towards a more convective regime, the distribution of total entropy generation becomes significantly affected. The presence of convection, driven by higher Ra_m values, leads to elevated fluid velocities and consequently, an increase in entropy production (*NS*). The regions experiencing the most pronounced temperature gradients, found near the heating and cooling zones, correspond to the areas with the highest *NS* values.

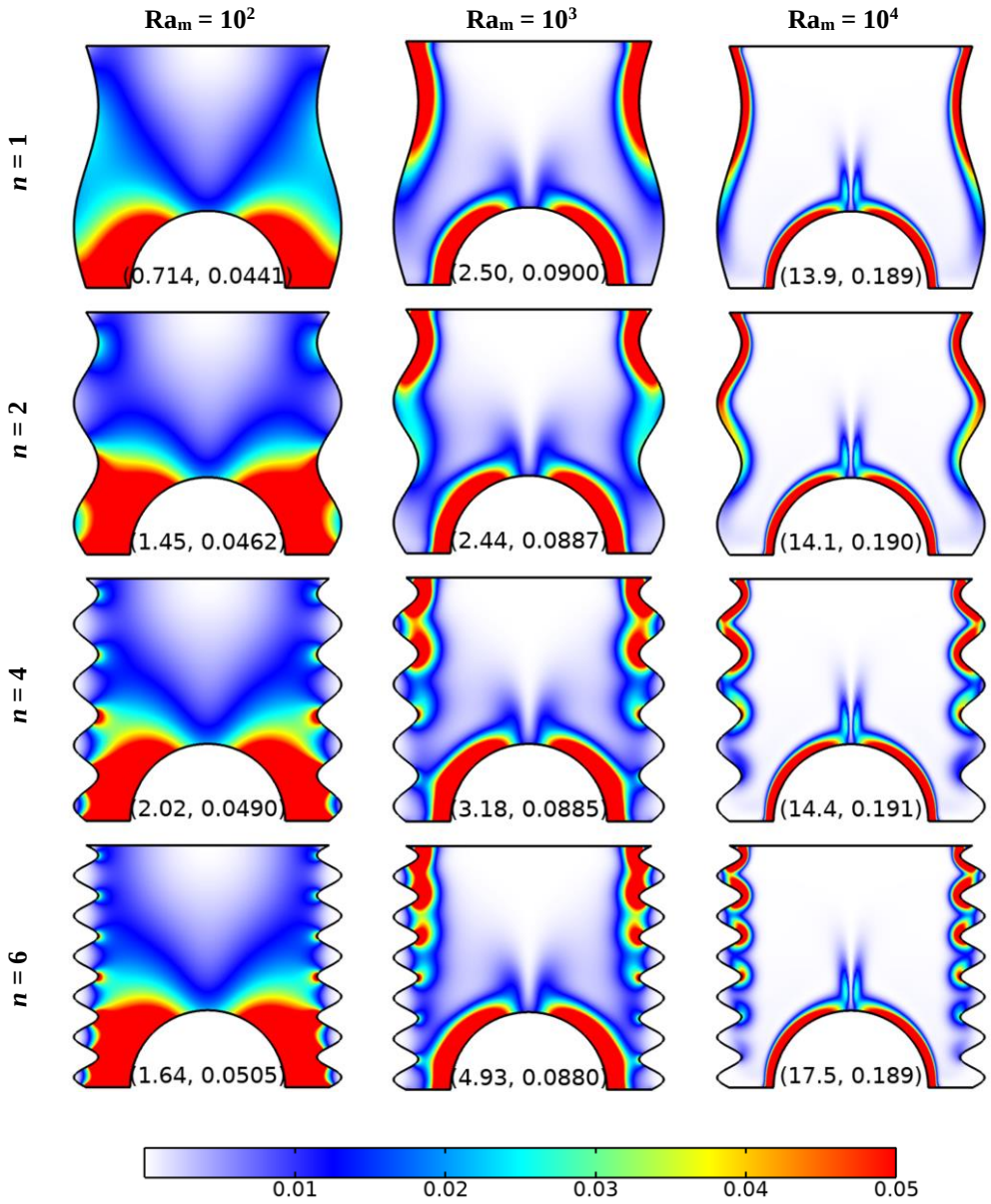

Fig. 12. Effect of Darcy-Rayleigh number Ra_m ($Ra_m = 10^2$ to 10^4) and n (n = 1, 2, 4 and 6) on normalized total irreversibility generation, for Da = 10^{-3} and Ha = 30. The values below each figure indicate NS_{max} and NS_{ave}, respectively.

Moving forward, Fig. 13 provides insights into the irreversibility generation resulting from viscous dissipation. Here, the interplay between various system parameters, such as Ra_m, n, Da and Ha, becomes apparent. As Ra_m increases, marking a shift towards stronger convective effects, the fluid velocity intensifies, contributing to increased entropy production due to viscous dissipation (NS_{vd}). The zones of heightened entropy generation become more concentrated along the active walls, emphasizing the complex interplay between thermal convection, magnetic fields, and viscous dissipation. Figure 14 further delves into the impact of the magnetic field (Ha) on irreversibility generation, highlighting the opposing role it plays in fluid circulation. As Ha values increase, the magnitude of magnetic field-induced irreversibility (NS_{mf}) experiences a corresponding rise. This behaviour underscores the significant influence of Ha on entropy generation and its crucial role in understanding the thermodynamic dynamics of the system.

In summary, entropy generation analysis provides invaluable insights into the multifaceted irreversibilities present in the thermal system. Higher Ra_m values intensify these irreversibilities due to the amplification of convection effects, while augmented magnetic fields enhance magnetic field-induced irreversibilities. Additionally, the Darcy number, which represents flow resistance within the porous medium, exerts a pivotal influence on the generation of irreversibilities. The intricate interplay of these multiphysical phenomena underscores the complexity of entropy generation and highlights its significance in discerning the hierarchy of thermodynamic irreversibilities within the system.

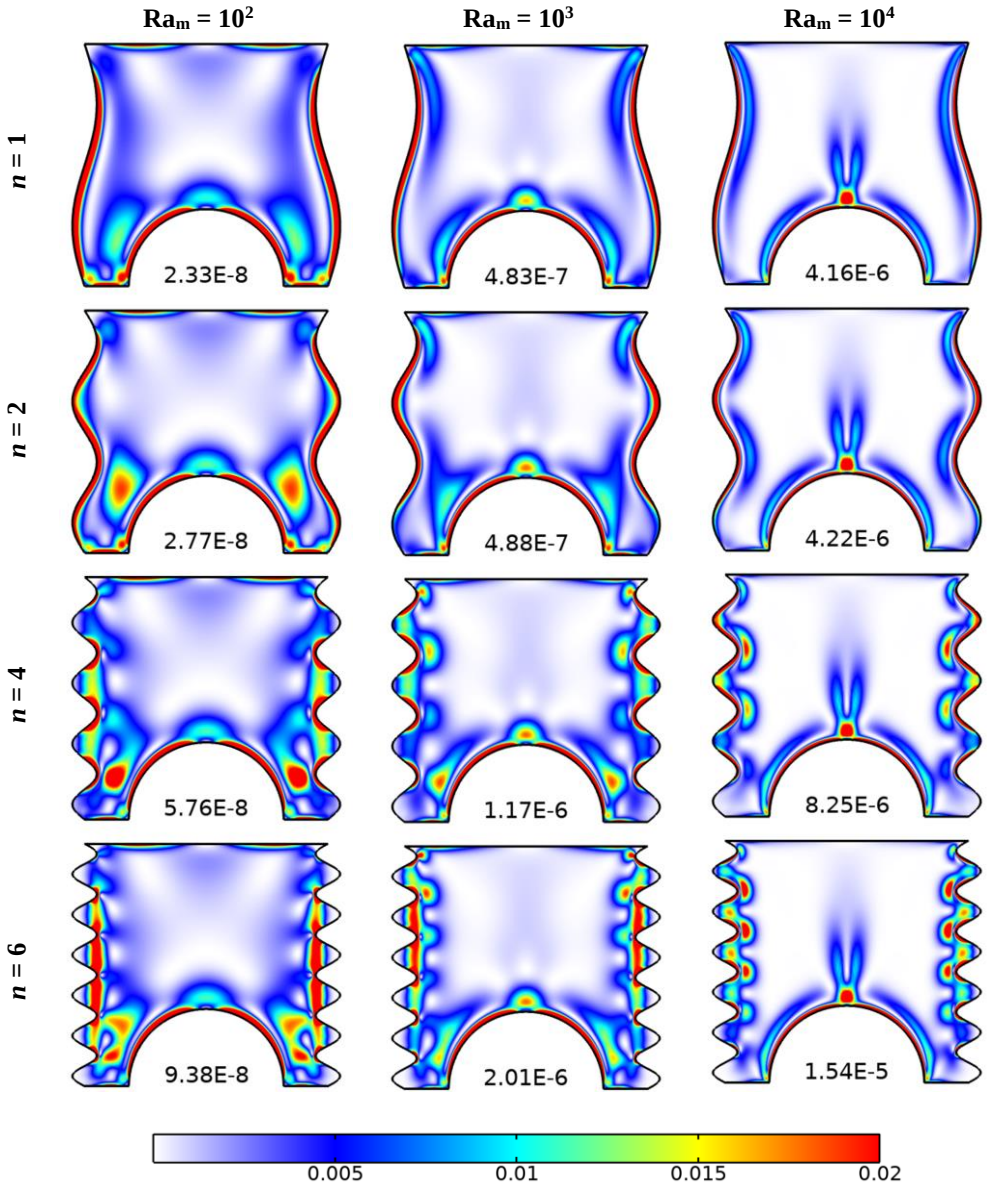

Fig. 13. Effect of Darcy-Rayleigh number (Ra_m = 10^2 to 10^4) and n (n = 1, 2, 4 and 6) on irreversibility generation due to viscous dissipation, for Da = 10^{-3} and Ha = 10. The value below each figure indicates maximum NS_{vd} (dimensionless).

This analysis not only contributes to a deeper understanding of the system's behaviour but also informs decisions in the design and optimization of thermally driven systems involving porous media and magnetic fields. Variations in heat transfer alteration are typically measured using the Nusselt number, as depicted in Fig. 15. It has been observed that the presence of undulations in wavy walls tends to enhance heat transfer, particularly at low Darcy-Rayleigh numbers, where conduction dominates. As Ra_m increases, Nu also increases, but the influence of the undulation number is not significant. In terms of the Darcy number, which represents flow resistance in porous media, higher Da values lead to reduced heat transfer due to the corresponding decrease in the fluid-based Rayleigh number. The impact of the undulation number on heat transfer in this context is not prominent. Regarding the Hartmann number, which affects fluid circulation and heat transfer, higher Ha values tend to dampen fluid flow, similar to the Darcy number, resulting in reduced heat transfer rates. However, it is worth noting that lower undulation levels exhibit better heat transfer under low Ha regimes.

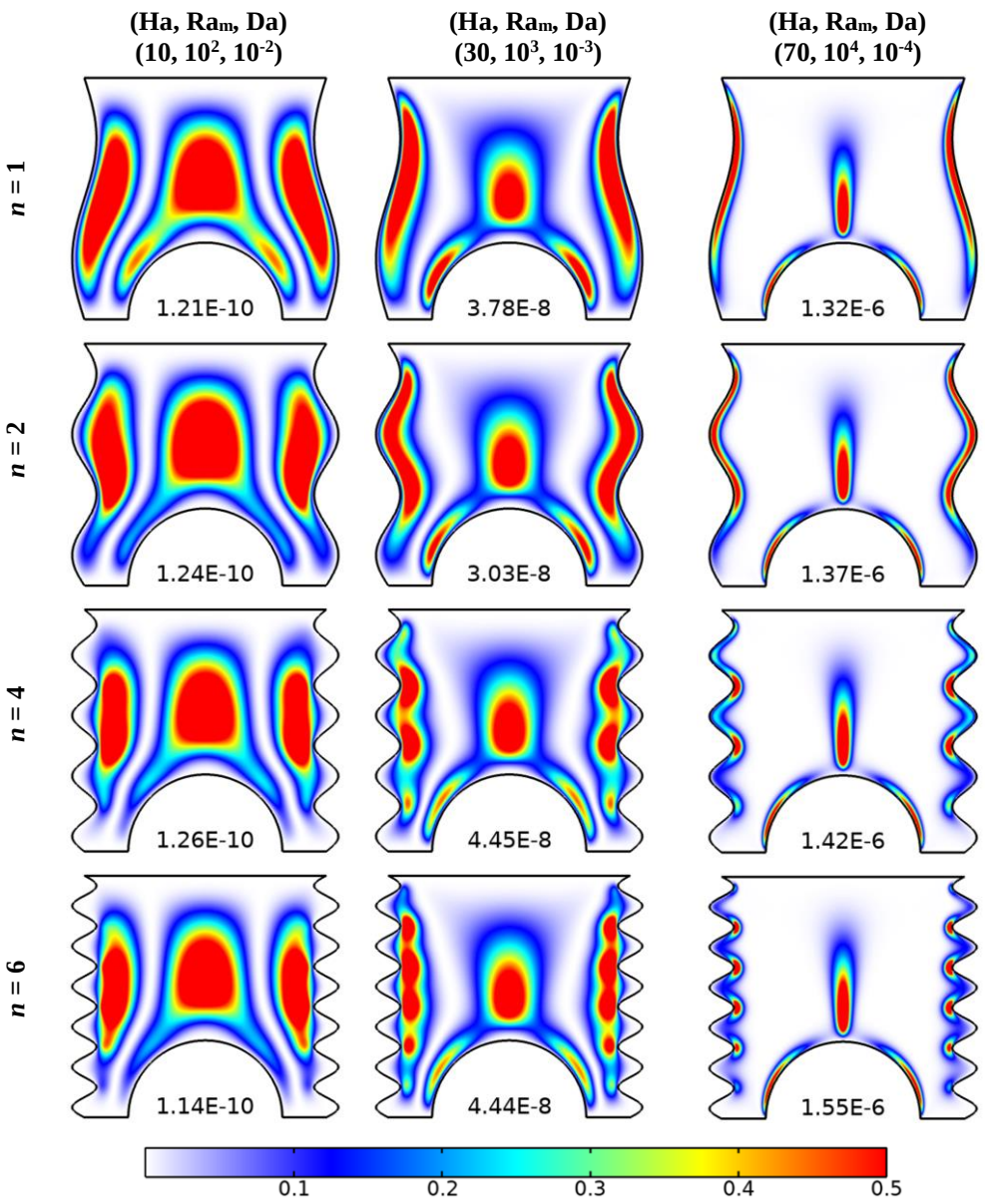

Fig. 14. Effect of Hartmann number (Ha = 10, 30, 70) and n (n = 1, 2, 4 and 6) on irreversibility generation due to magnetic field. The value below each figure indicates maximum NS_{mf} (dimensionless).

Entropy generation, represented by the irreversibility (*NS*), is depicted for all considered cases in Fig. 16. Higher values of the Darcy-Rayleigh number exacerbate irreversibility due to increased convection effects, whereas elevated magnetic fields and Darcy numbers lead to a reduction in irreversibility. At higher Ra_m values, greater undulations exhibit increased irreversibility. Moreover, more undulations result in higher irreversibility across all considered Hartmann and Darcy values.

5. Concluding remarks

This work comprehensively explores the intricate interplay of multiple physical parameters that govern thermal transport and entropy generation in a complex enclosure. This investigation has provided valuable insights and noteworthy findings that contribute to the understanding of thermal systems involving porous media and magnetic fields. Here, we summarize the key conclusions drawn from this research:

It is observed that the undulations in the wavy walls significantly influence the flowing fluid and heat transfer patterns within the enclosure. The undulations not only alter the flow direction but also enhance heat transfer due to the increased surface area, with optimum heat transfer occurring at specific undulation values.

This study has shown that the Darcy number, representing flow resistance within the porous domain, plays a crucial role in governing fluid flow and heat transfer. Surprisingly, higher Da values, which should theoretically allow for increased flow, led

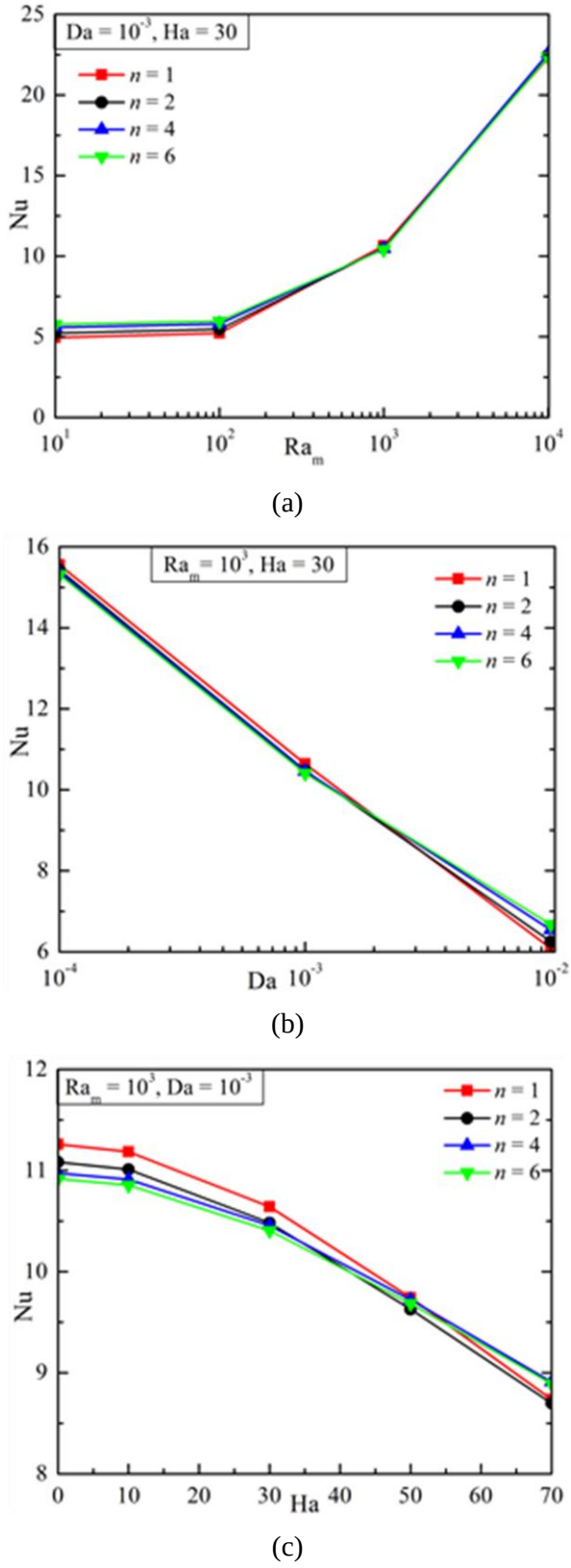

Fig. 15. Average Nu for the various undulation parameters (n) for changing (a) Ra_m (= 1–10^4) when Da = 10^{-3}, Ha = 30, (b) Da (=10^{-4}–10^{-2}) when Ra_m = 10^3, Ha = 30, and (c) Ha (= 0–70) when Ra_m = 10^3, Da = 10^{-3}.

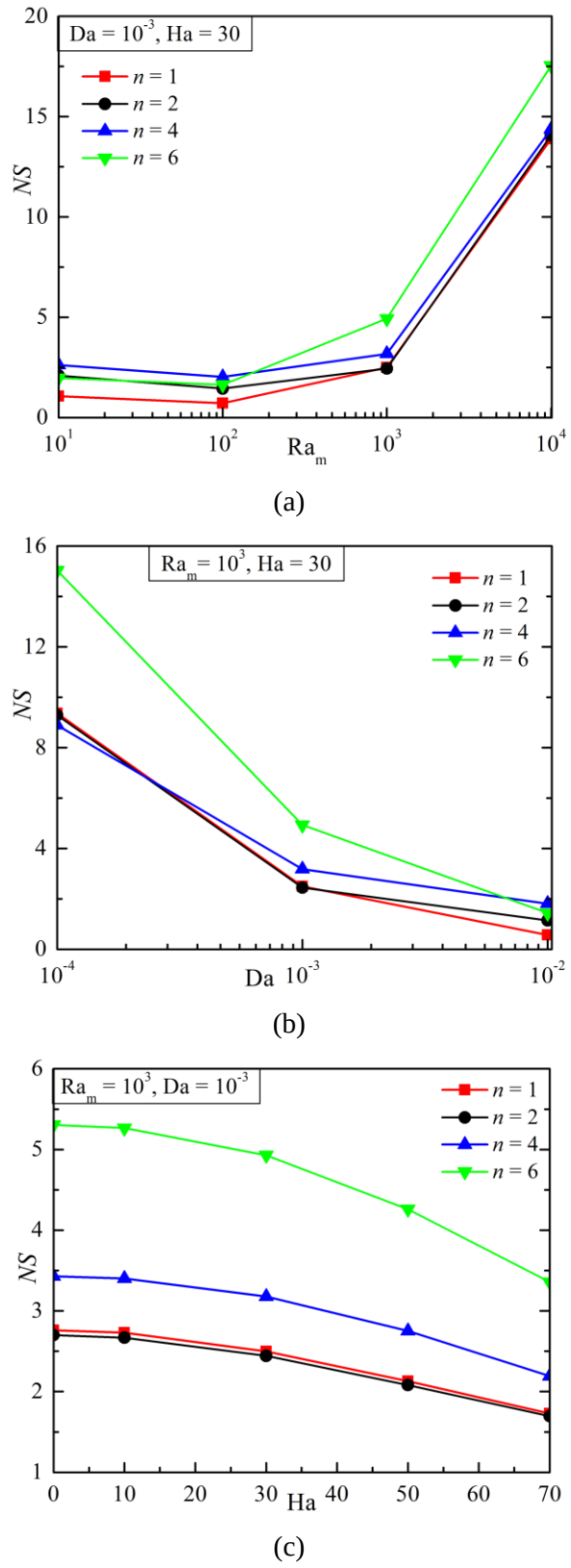

Fig. 16. Total *NS* for the various undulation parameters (n) for changing (a) Ra_m (= 1–10^4) when Da = 10^{-3}, Ha = 30, (b) Da (=10^{-4}–10^{-2}) when Ra_m = 10^3, Ha = 30, and (c) Ha (= 0–70) when Ra_m = 10^3, Da = 10^{-3}.

to reduced flow rates and heat transfer due to the reduced fluid-based Rayleigh number (Ra).

The existence of an external magnetic field, quantified by the Hartmann number, impacts fluid circulation and heat transfer. Higher Ha values dampen fluid flow, leading to changes in circulation patterns and altered heat transfer rates.

Present findings elucidate the intriguing flow signatures and heatline patterns within the cavity. We have noted the formation of distinctive circulation patterns depending on the heater-cooler positions, leading to variations in flow direction and velocity magnitude. Heatlines have revealed the transition from conduction-dominated to convection-dominated heat transfer as the Darcy-Rayleigh number increases.

The analysis of entropy generation has provided valuable insights into the irreversibilities present in the thermal system. Higher Ra_m values intensify these irreversibilities due to stronger convection effects, while elevated magnetic fields enhance magnetic field-induced irreversibilities. The Darcy number has been identified as a key parameter influencing entropy generation.

In summary, the findings of this study imply that the fluid flow and heat transport phenomena in a thermal system are strongly influenced by the shape of the heating, as well as cooling surfaces. Such findings are very effective for designing a compact heat exchanger, chemical reactor, bio-microfluidic devices, etc. The current research might be expanded into three-dimensional models under various boundary conditions for unstable fluid flow.

Data availability statement

The data that support the findings of this study are available from the corresponding author upon reasonable request.

References

[1] Hartmann, J. (1937). Hg-dynamics I. Theory of the laminar flow of an electrically conductive liquid in a homogeneous magnetic field. *Det Kgl. Danske Vidensk-abernes Selskab. Mathematisk-fysiske Meddelelser*, 15(6).

[2] Manna, N.K., & Biswas, N. (2021). Magnetic force vectors as a new visualization tool for MHD convection. *International Journal of Thermal Sciences*, 167, 107004. doi: 10.1016.j.ijthermalsci.2021.107004

[3] Barnothy, M.F. (ed) (1964). *Biological Effects of Magnetic Fields*. Plenum Press. New York

[4] Rashidi, S., Esfahani, J.A., & Maskaniyan, M. (2017). Applications of magnetohydrodynamics in biological systems – a review on the numerical studies. *Journal of Magnetism and Magnetic Materials*, 439, 358–372. doi: 10.1016/j.jmmm. 2017.05.014

[5] Ozoe, H.(2005). *Magnetic Convection*. Imperial College Press, Singapore.

[6] Ganguly, R., Sen, S., & Puri, I.K. (2004). Thermomagnetic convection in a square enclosure using a line dipole. *Physics of Fluids*, 16(7), 2228–2236. doi: 10.1063/1.1736691

[7] M'hamed, B., Sidik, N.A.C., Yazid, M.N.A.W.M., Mamat, R., Najafi, G., & Kefayati, G.H.R. (2016). A review on why researchers apply external magnetic field on nanofluids. *International Communications in Heat and Mass Transfer*, 78, 60–67. doi: 10.1016/j.icheatmasstransfer.2016.08.023

[8] Manna, N.K., Mondal, C. Biswas, N., Sarkar, U.K., Öztop, H.F., & Abu-Hamdeh, N.H. (2021). Effect of multibanded magnetic field on convective heat transport in linearly heated porous systems filled with hybrid nanofluid. *Physics of Fluids*, 33, 053604. doi: 10.1063/5.0043461

[9] Kabeel, A.E., El-Said, E.M.S., & Dafea, S.A. (2015). A review of magnetic field effects on flow and heat transfer in liquids: Present status and future potential for studies and applications. *Renewable and Sustainable Energy Reviews*, 45, 830–837. doi: 10.1016/j.rser.2015.02.029

[10] Khaled, A.-R.A., & Vafai, K. (2003). The role of porous media in modeling flow and heat transfer in biological tissues. *International Journal of Heat and Mass Transfer*, 46(26), 4989–5003. doi: 10.1016/S0017-9310(03)00301-6

[11] Manna, N.K., Mondal, M.K., & Biswas, N. (2021). A novel multi-banding application of magnetic field to convective transport system filled with porous medium and hybrid nanofluid. *Physica Scripta*, 96(6), 065001. doi: 10.1088/1402-4896/abecbf

[12] Shenoy, A., Sheremet, M., & Pop. I. (2016). *Convective flow and heat transfer from wavy surfaces. Viscous fluids, porous media and nanofluids*, CRC Press, Taylor & Francis Group, New York. doi: 10.1201/9781315367637

[13] Dalal, A., & Das, M.K. (2006). Natural convection in a cavity with a wavy wall heated from below and uniformly cooled from the top and both sides. *ASME Journal of Heat and Mass Transfer* 128(7), 717–725. doi: 10.1115/1.2194044

[14] Cheong, H.T., Sivasankaran, S., & Bhuvaneswari, M. (2017). Natural convection in a wavy porous cavity with sinusoidal heating and internal heat generation. *International Journal of Numerical Methods for Heat & Fluid Flow*, 27(2), 287–309. doi: 10.1108/HFF-07-2015-0272

[15] Al-Srayyih, B.M., Gao, S., & Hussain, S.H. (2019). Natural convection flow of a hybrid nanofluid in a square enclosure partially filled with a porous medium using a thermal non-equilibrium model. *Physics of Fluids*, 31, 043609. doi: 10.1063/1.5080671

[16] Babar, H., Sajid, M.U., & Ali, H.M. (2019). Viscosity of hybrid nanofluids: A critical review. *Thermal Science*, 23(3B), 1713–1754. doi: 10.2298/TSCI181128015B

[17] Sarkar, J., Ghosh, P., & Adil, A.(2015). A review on hybrid nanofluids: Recent research, development and applications. *Renewable and Sustainable Energy Reviews*. 43, 164–177. doi: 10.1016/j.rser.2014.11.02 3

[18] Kasaeian, A., Daneshazarian, R., Mahian, O., Kolsi, L., Chamkha, A.J., Wongwises, S., & Pop, I.(2017). Nanofluid flow and heat transfer in porous media: A review of the latest developments. *International Journal of Heat and Mass Transfer*, 107, 778–791. doi: 10.1016/j.ijheatmasstransfer.2016.11.074

[19] Biswas, N., Mandal, D.K., Manna, N.K.,. Gorla, R.S.R., & Chamkha, A.J. (2021). Magnetohydrodynamic thermal characteristics of water-based hybrid nanofluid filled non-Darcian porous wavy enclosure: effect of undulation. *International Journal of Numerical Methods for Heat & Fluid Flow*, 32(5), 11742−1777. doi: 10.1108/HFF-03-2021-0190

[20] Biswas, N., Manna, N.K., Chamkha, A.J. & Mandal, D.K. (2021). Effect of surface waviness on MHD thermo-gravitational convection of $Cu-Al_2O_3$−water hybrid nanofluid in a porous oblique enclosure. *Physica Scripta*, 96(10), 105002. doi: 10.1088/1402-4896/ac0f94

[21] Mandal, D.K., Biswas, N., Manna, N.K., Gorla, R.S.R., & Chamkha, A.J. (2022). Magneto-thermal convection of hybrid nanofluid in a non-Darcian porous complex wavy enclosure. *The European Physical Journal Special Topics*, 231, 2695–2712. doi: 10.1140/epjs/s11734-022-00595-6

[22] Biswas, N., Mondal, M.K., Mandal, D.K., Manna, N.K., Gorla, R.S.R., & Chamkha, A.J. (2022). A narrative loom of hybrid nanofluid filled wavy walled tilted porous enclosure imposing a partially active magnetic field. *International Journal of Mechanical Sciences*, 217, 107028. doi: 10.1016/j.ijmecsci.2021.107028

[23] Bahmani, M., Babagoli, M., Jalili, P., Jalili, B., & Ganji, D.D. (2024).The numerical study on the MHD natural convection trend of square/circle corrugated porous media. *Journal of Engineering Research* (in press). doi. 10.1016/j.jer.2024.05.012

[24] Hamid, M., Usman, M., Khan, W.A., Haq, R.U., & Tian, Z. (2024). Characterizing natural convection and thermal behavior in a square cavity with curvilinear corners and central circular obstacles. *Applied Thermal Engineering*, 248(A), 123133. doi: 10.1016/j.applthermaleng.2024.123133

[25] Pandit, S., Mondal, M.K., Manna, N.K., Sanyal, D., Biswas, N., & Mandal, D.K. (2024). Synergistic effects of multi-segmented magnetic fields, wavy-segmented cooling, and distributed heating on hybrid nanofluid convective flow in tilted porous enclosures. *International Journal of Thermofluids*, 4, 100826. doi: 10.1016/j.ijft.2024.100826

[26] Guedri, K., Zaim, A.N., Sajadi, S.M., Jasim, D.J., Aissa, A., Salahshour, S., Almuhtady, A., Younis, O., Baghaei, S., & Al-Kouz, W. (2024). Investigation of free convection in a wavy trapezoidal porous cavity with MWCNT-Fe_3O_4/Water hybrid nanofluid under MHD effects: Galerkin finite element analysis. *Case Studies in Thermal Engineering*, 56, 104243. doi: 10.1016/j.csite.2024.104243

[27] Mandal, D.K., Mondal, M.K., Biswas, N., Manna, N.K., Al-Farhany, K., Mitra, A., & Chamkha, A.J. (2024). Convective heat transport in a porous wavy enclosure: nonuniform multi-frequency heating with hybrid nanofluid and magnetic field. *Heliyon*, 10 (9), e29846. doi: 10.1016/j.heliyon.2024.e29846

[28] Al-Dulaimi, Z., Kadhim, H.T., Jaffer, M.F., Al-Manea, A., Al-Rbaihat, R., & Alahmer, A. (2024). Enhanced conjugate natural convection in a corrugated porous enclosure with Ag-MgO hybrid nanofluid. *International Journal of Thermofluids*, 21, 100574. doi: 10.1016/j.ijft.2024.100574

[29] Said, M.A., Togun, H., Abed, A.M., Biswas, N., Mohammed, H.I., Sultan, H.S., Mahdi, J.M., & Talebizadehsardari, P. (2024). Evaluation of wavy wall configurations for accelerated heat recovery in triplex-tube energy storage units for building heating applications. *Journal of Building Engineering*, 94, 109762. doi: 10.1016/j.jobe.2024.109762

[30] Manna, N.K., Saha, A., Biswas, N., & Ghosh, K. (2024). Shape matters: Convection and entropy generation in magneto-hydrodynamic nanofluid flow in constraint-based analogous annular thermal systems. *Numerical Heat Transfer, Part A: Applications*, 1−33. doi: 10.1080/10407782.2024.2347585

[31] Chatterjee, D., Biswas, N., Manna, N.K., & Mandal, D.K. (2023). Magneto-nanofluidic convection and entropy generation in discretely heated cylindrical annuli with central conducting obstructions. *Journal of Magnetism and Magnetic Materials*, 569, 170442. doi: 10.1016/j.jmmm.2023.170442

[32] Maxwell, J. (1904). *A treatise on electricity and magnetism* (2nd ed.). Oxford University Press, Cambridge.

[33] Brinkman, H.C. (1952). The viscosity of concentrated suspensions and solutions. *The Journal of Chemical Physics*, 20(4), 571−580. doi: 10.1063/1.1700493

[34] Chatterjee, D., Biswas, N., Manna, N.K., & Sarkar, S. (2023). Effect of discrete heating-cooling on magneto-thermal-hybrid nanofluidic convection in cylindrical system. *International Journal of Mechanical Science*, 238, 107852. doi: 10.1016/j.ijmecsci.2022.107852

[35] Halder, A., Bhattacharya, A., Biswas, N., Manna, N.K., & Mandal, D.K. (2024). Convective heat transport and entropy generation in butterfly-shaped magneto-nanofluidic systems with bottom heating and top cooling. *International Journal of Numerical Methods for Heat & Fluid Flow*, 34(2), 837−877. doi: 10.1108/HFF-06-2023-0353

[36] Suresh, S, Venkitaraj, K, Selvakumar, P, & Chandrasekar, M. (2012). Effect of Al_2O_3–Cu/water hybrid nanofluid in heat transfer. *Experimental Thermal and Fluid Science*, 38, 54–60. doi: 10.1016/j.expthermflusci.2011.11.007

[37] Biswas, N., Chatterjee, D., Sarkar, S., & Manna, N.K. (2024). Magneto-nanofluidic thermal transport and irreversibility in semicircular systems with heated wavy bottom under constant fluid volume and cooling surface constraints. *International Journal of Numerical Methods for Heat & Fluid Flow*, 34(2), 1021−1059. doi: 10.1108/HFF-06-2023-0354

[38] Ghasemi, B., Aminossadati, S.M., & Raisi, A. (2011). Magnetic field effect on natural convection in a nanofluid-filled square enclosure. *International Journal of Thermal Sciences*, 50(9), 1748–1756. doi: 10.1016/j.ijthermalsci.2011.04.010

[39] Pandit, S., Mondal, M.K., Manna, N.K., Sanyal, D., Biswas, N., & Mandal, D.K. (2024). Synergistic effects of multi-segmented magnetic fields, wavy-segmented cooling, and distributed heating on hybrid nanofluid convective flow in tilted porous enclosures. *International Journal of Thermofluids*, 24, 100826. doi: 10.1016/j.ijft.2024.100826